

# **1A simplified Permafrost-Carbon model for long-term 2climate studies with the CLIMBER-2 coupled earth system 3model**

4

**5K.A. Crichton <sup>1,2</sup>, D.M. Roche <sup>3,4</sup>, G. Krinner <sup>1,2</sup> and J. Chappellaz <sup>1,2</sup>**

6[1] {CNRS, LGGE (UMR5183), F-38041 Grenoble, France}

7[2] {Univ. Grenoble Alpes, LGGE (UMR5183), F-38041 Grenoble, France}

8[3] {CEA/INSU-CNRS/UVSQ, LSCE (UMR8212), Centre d'Etudes de Saclay CEA-Orme  
9des Merisiers, bat. 701 91191 Gif-sur-Yvette Cedex, France}

10[4] {Cluster Earth and Climate, Department of Earth Sciences Faculty of Earth and Life  
11Sciences, Vrije Universiteit Amsterdam De Boelelaan 1085, 1081 HV Amsterdam, The  
12Netherlands}

13Correspondence to: K.A. Crichton (kcrichton@lgge.obs.ujf-grenoble.fr)

14

## **15Abstract**

16We present the development and validation of a simplified permafrost-carbon mechanism for  
17use with the land surface scheme operating in the CLIMBER-2 earth system model. The  
18simplified model estimates the permafrost fraction of each grid cell according to the balance  
19between modelled cold (below 0°C) and warm (above 0°C) days in a year. Areas diagnosed as  
20permafrost are assigned a reduction in soil decomposition rate, thus creating a slow  
21accumulating soil carbon pool. In warming climates, permafrost extent reduces and soil  
22decomposition rates increase, resulting in soil carbon release to the atmosphere. Four  
23accumulation/decomposition rate settings are retained for experiments within the CLIMBER-  
242(P) model, which are tuned to agree with estimates of total land carbon stocks today and at  
25the last glacial maximum. The distribution of this permafrost-carbon pool is in broad  
26agreement with measurement data for soil carbon content. The level of complexity of the  
27permafrost-carbon model is comparable to other components in the CLIMBER-2 earth system  
28model.

## 21 Introduction

3 Model projections of climate response to atmospheric CO<sub>2</sub> increases predict that high northern  
 4 latitudes experience amplified increases in mean annual temperatures compared to mid-  
 5 latitudes and the tropics (Collins et al., 2013). The large carbon pool locked in permafrost  
 6 soils of the high northern latitudes (Tarnocai et al., 2009) and its potential release on thaw  
 7 (Schuur et al, 2008, Harden et al, 2012) make permafrost and permafrost related carbon an  
 8 important area of study. Thus far permafrost models that have been coupled within land-  
 9 surface schemes have relied on thermal heat diffusion calculations from air temperatures into  
 10 the ground to diagnose permafrost location and depth within soils (Koven et al., 2009, Wania  
 11 et al., 2009a, Dankers et al., 2011, Ekici et al., 2014). This approach requires a good physical  
 12 representation of topography, soil types, snow cover, hydrology, soil depths and geology to  
 13 give a reliable output (Riseborough et al, 2008). The physically based approach lends itself to  
 14 smaller grid cells and short timescale snapshot simulations for accuracy of model output. The  
 15 aim of this work is to develop a simplified permafrost-carbon mechanism that is suitable for  
 16 use within the CLIMBER-2 earth system model (Petoukhov et al., 2000, Ganopolski et al.,  
 17 2001), and also suitable for long timescale experiments. The CLIMBER-2 model with a  
 18 coupled permafrost-carbon mechanism, combined with proxy marine, continental and ice core  
 19 data provide a means to model the past dynamic contribution of permafrost-carbon within the  
 20 carbon cycle.

21

### 221.1 Physical permafrost modelling

23 Several land surface models diagnose permafrost and concomitant higher soil carbon  
 24 concentrations (Wania et al., 2009a,b, Koven et al., 2009, Dankers et al., 2011). These models  
 25 are usually driven with climatic variables output from global climate models (GCMs) and grid  
 26 cell sizes are the order of 2.5° (the order of hundreds of km) for global simulations. These  
 27 models use surface air temperature and thermal diffusion calculations to estimate the soil  
 28 temperature at depths, and from this the depth at which water freezes in the soil. An active  
 29 layer thickness (ALT) can be determined from this, and soil carbon dynamics are calculated  
 30 for the unfrozen parts of the soil. These land surface models may also include a representation  
 31 of peatlands (Sphagnum dominated areas, and wetlands), which store an estimated 574 GtC in

1 northern peatlands (Yu et al., 2010), of which a large part are located within the permafrost  
2 region (Northern Circumpolar Atlas: Jones et al., 2009). The dynamic response of carbon in  
3 permafrost soils subject to (rapid) thaw is not well constrained (Schuur et al., 2011) and field  
4 studies and modelling studies still seek to better constrain this. Riseborough et al. (2008)  
5 reviewed advances in permafrost modelling identifying that modelling of taliks (pockets or  
6 layers of thawed soil at depth which do not refreeze in winter) complicates physical  
7 modelling. The importance of soil depth (lower boundary conditions) was also highlighted,  
8 Alexeev et al. (2007) demonstrated that the longer the simulation, the larger the soil column  
9 depth required in order to produce reliable thermal diffusion-based temperature calculations:  
10 A 4m soil depth can produce reliable temperature predictions for a 2-year simulation, and for  
11 a 200-year simulation a 30m soil depth would be required. Van Huissteden and Dolman  
12 (2012) reviewed Arctic soil carbon stocks estimates and the permafrost-carbon feedback.  
13 They note the processes by which carbon loss occurs from thawing permafrost including  
14 active layer thickening (also caused by vegetation disturbance), thermokarst formation,  
15 dissolved organic carbon (DOC) export, fire and other disturbances. Their conclusions were  
16 that "current models are insufficiently equipped to quantify the carbon release at rapid thaw of  
17 ice-rich permafrost" which within a model would require accurate representation of local  
18 topography, and hydrology as well as a-priori knowledge of the ice-content in the soils.  
19 Koven et al. (2013) further highlighted the importance of soil depths and of soil and snow  
20 dynamics on the accuracy of permafrost extent in CMIP (coupled model intercomparison  
21 project) models. The high computing power requirements of physical models at grid sizes  
22 where output could be an acceptable confidence level makes these kind of models currently  
23 unsuitable for long timescale dynamically coupled modelling studies. Current CMIP model  
24 projections of future climate reported by the IPCC (Stocker et al., 2013) do not include a  
25 possible feedback mechanism from permafrost-soils. There exists some studies of the possible  
26 future response of carbon in soils of the permafrost zone which do not rely on heat diffusion  
27 calculations down the soil column (Scheafer et al 2011, Harden et al 2012, Schneider von  
28 Diemling et al 2012). However, these kind of treatments are not suitable for the study of  
29 paleoclimate as they require a-priori knowledge of soil organic carbon content (socc) of the  
30 soils at relatively high resolution. This is currently not yet feasible when considering last  
31 glacial maximum soils (for example).

32

## 11.2 Past permafrost carbon

Zimov et al. (2009) created a physical model for carbon dynamics in permafrost soils. This 3dimensional model was intended to simulate the carbon dynamics specifically in the 4permafrost region. Carbon input to the soil originates from root mortality and aboveground 5litter transport via organic carbon leaching and mixing by bioturbation and cryoturbation. 6Loss of carbon from the soils occurs via decomposition. The frozen soil active layer depth 7also determines the maximum root depth of vegetation. Modelled soil carbon profiles were 8similar to those found in present day ground data for similar conditions. Results of 9experiments where the temperature zone was changed linearly from Temperate to Cold, then 10snapped back to Temperate (mimicking a glaciation then termination in Europe) demonstrated 11the characteristic of slow carbon accumulation in permafrost soils, and fast carbon release on 12thaw. An important result of this study was that the main driver of the high carbon content in 13the frozen soils was the low decomposition rates, which reduce further with depth in the soil 14column, as a result of permafrost underlying an active layer which cycles between freezing 15and thawing in the year. To estimate the amounts of carbon stored on the land and the ocean 16at LGM, Ciais et al. (2012) used  $\delta^{18}\text{O}$  data and carbon cycle modelling to calculate gross 17primary productivity (GPP) at LGM and in the present day. They estimate that the total land 18carbon stocks had increased by 330GtC since LGM, but that 700GtC less was presently stored 19as inert land carbon stocks compared to LGM. Zech et al. (2011) studying two permafrost- 20loess paleosol sequences concluded that on glacial timescales the effect of reduced biomass 21productivity may be of secondary importance to the effect of permafrost preserving soil 22organic matter when considering total land carbon stocks. The Ciais et al. (2012) inert land 23carbon stock may represent this permafrost carbon pool.

24

## 251.3 Carbon cycle responses during a deglaciation

26The current leading hypothesis for the fast rise in atmospheric  $\text{CO}_2$  in the last glacial 27termination (17.5kyr to 12kyr BP) (Monnin et al., 2001) is that carbon was outgassed from the 28ocean via a reorganisation of ocean circulation that released a deep carbon store in the 29Southern ocean (Sigman et al., 2010, Fischer et al., 2010, Shakun et al., 2012). The Zimov et 30al. (2009) model, Ciais et al. (2012) and the  $\delta^{13}\text{CO}_2$  record for the last termination (Lourantou 31et al., 2010, Schmitt et al., 2012) suggest that permafrost may have had a role to play in the

1 dynamics of the carbon cycle during the last termination. At the start of glacial termination 1  
2 (from the end of the last glacial period, the transition to the interglacial climate, starting at  
3 ~17.5 kyrBP) a fast drop in the  $\delta^{13}\text{CO}_2$  of the atmosphere was seen from ice core data. Soil  
4 carbon has a  $\delta^{13}\text{C}$  signature depleted by around 18‰ compared to the atmosphere (Maslin and  
5 Thomas, 2003), a release of carbon from thawing permafrost soils is a possible explanation  
6 for the  $\delta^{13}\text{CO}_2$  record.

7 In this study, we aim to develop a permafrost-carbon model for long-term paleoclimate  
8 studies. We present the development of the permafrost-carbon model and validate it with  
9 present-day ground measurement data for soil carbon concentrations in high northern latitude  
10 soils.

11

## 12 **2 Model development**

### 13 **2.1 CLIMBER-2 standard model**

14 The CLIMBER-2 model (Petoukhov et al., 2000, Ganopolski et al., 2001) consists of a  
15 statistical-dynamical atmosphere, a 3-basin averaged dynamical ocean model with 21 vertical  
16 uneven layers and a dynamic global vegetation model, VECODE (Brovkin et al., 1997). The  
17 model version we use is as Bouttes et al. (2012) and Brovkin et al. (2007). The model can  
18 simulate around 20 kyr in 10 hours (on a 2.5 GHz processor) and so is particularly suited to  
19 palaeoclimate and long timescale fully coupled modelling studies. The version of CLIMBER-  
20 we use (Bouttes et al., 2009, 2012) is equipped with a carbon-13 tracer, ice sheets and deep  
21 sea sediments (allowing the representation of carbonate compensation) in the ocean (Brovkin  
22 et al. 2007) as well as ocean biogeochemistry. The ice sheets are determined by scaling ice  
23 sheets size between the Last Glacial Maximum (LGM) condition from Peltier (2004) and the  
24 Pre-Industrial (PI) ice sheet using the sea level record to determine land ice volume (Bouttes  
25 et al. 2012). The dynamic vegetation model has two plant functional types (PFTs); trees and  
26 grass, plus bare ground as a dummy type. It has two soil pools; “fast” and “slow” representing  
27 litter and humus respectively. Soils have no depth, and are only represented as carbon pools.  
28 The carbon pools of the terrestrial vegetation model are recalculated once every year. The grid  
29 cell size of the atmospheric and land surface models are approximately  $51^\circ$  longitude ( $360/7$   
30 degrees) by  $10^\circ$  latitude. Given the long time-scale applications of the CLIMBER-2 model  
31 and the very large grid size for both atmosphere and land, none of the existing approaches of

1modelling permafrost-carbon are suitable. Thermal diffusion based physical models would  
2produce results with unacceptable uncertainties (error bounds) compounding over long  
3timescales. To create the permafrost model for CLIMBER-2, the driving mechanism creating  
4high soil carbon concentrations is a reduced soil decomposition rate in the presence of  
5permafrost, identified by Zimov et al. (2009) as the primary driver in soil carbon  
6accumulation for these soils.

## 72.2 Permafrost-carbon mechanism

8CLIMBER-2 grid cells for the land surface model are very large. Two options are available to  
9diagnose permafrost location: either by creating a sub-grid within the land grid or by  
10diagnosing a fraction of each grid cell as permafrost which is the approach followed here.  
11Conceptually the sub-grid model represents keeping permafrost-carbon separate from other  
12soil carbon, and the re-mixing model represents mixing all soil carbon in a grid cell. Figure 1  
13shows a schematic representation of a CLIMBER-2 grid cell, and how the permafrost fraction  
14of the land is defined relative to other cell parameters when permafrost is diagnosed as a  
15fraction of each cell. For the carbon cycle the calculations of carbon fluxes between  
16atmosphere and land grid cells are for the cell mean. Each grid cell contains cell-wide soil-  
17carbon pools (fast soil or slow soil, per plant functional type), so to account for permafrost-  
18soils either a new permafrost-soil pool needs to be created for each grid cell, or permafrost  
19soils can be mixed back into the standard soil pools at every time-step (Fig. 2a). If the land  
20grid is downscaled a third option is available, where each sub-grid cell maintains an  
21individual soil carbon pool (Fig. 2b). This, however, requires an increase in computational  
22time which slows down the run speed of the model.

23The soil carbon in CLIMBER-2 is built from vegetation mortality and soil carbon  
24decomposition is dependent on surface air temperature, the total amount of carbon in the  
25pool and the source of carbon (i.e. trees or grass). Equation 1 shows how carbon content of  
26each pool is calculated in CLIMBER-2. The pool is denoted by  $C_i$  where pool  $C_1$  is plant  
27green phytomass (leaves),  $C_2$  is plant structural biomass (stems and roots),  $C_3$  is a soil pool  
28made of litter and roots residue and finally  $C_4$  is a soil pool made of humus and residues of  
29woody-type stems and roots. Hereafter, the soil pools will be referred to as  $\text{Soil}_{\text{fast}}$  for  $C_3$  and  
30 $\text{Soil}_{\text{slow}}$  for  $C_4$ . The equations (eq. 1) are numerically solved in the model with a timestep of  
31one year.

$$\begin{aligned}
1 \quad \frac{dC_1^p}{dt} &= k_1^p N - m_1^p C_1^p \\
2 \quad \frac{dC_2^p}{dt} &= (1 - k_1^p) N - m_1^p C_2^p \\
3 \quad \frac{dC_3^p}{dt} &= k_2^p m_1^p + k_3^p m_2^p C_2^p - m_3^p C_3^p \\
4 \quad \frac{dC_4^p}{dt} &= k_4^p m_2^p C_2^p + k_5^p m_3^p C_3^p - m_4^p C_4^p
\end{aligned} \tag{1}$$

5

6where

7C is the carbon content in the pool (kgC/m<sup>2</sup>)

8k are allocation factors (0 < k<sub>i</sub> < 1)

9N is net primary productivity (kgC/m<sup>2</sup>/yr)

10m<sub>i</sub> are decomposition rates for the carbon in each pool, (/yr)

11p is the plant functional type (trees or grass)

12

13The residence time of carbon in soil pools is 1/m, we call this τ. For soil carbon pools C<sub>3</sub> and

14C<sub>4</sub>, tau is:

$$15 \quad \tau_i = n_i^p \cdot e^{(-ps5(T_{mat} - T_{ref}))}, \tag{2}$$

16

17where

18i is the soil pool

19n is a multiplier dependent on the pool type

20ps5 is a constant, = 0.04

21T<sub>mat</sub> is mean annual temperature at the surface-air interface, °C

22T<sub>ref</sub> is a reference soil temperature, fixed in CLIMBER-2 at 5°C

23

The value of  $n$  is dependent upon the soil carbon type, being 900 for all slow soils, 16 for fast tree PFT (plant functional type) soil and 40 for fast grass PFT soil. The decomposition rates for organic residue in the soils are most strongly based on soil microbial activity and the relative amount of lignin in the residues (Aleksandrova 1970, Brovkin et al., 1997). Increasing the residence time of carbon in permafrost affected soils reduces the decomposition rates and results in higher soil carbon concentrations. We modify the residence time,  $\tau_{3,4}$ , in the presence of permafrost using:

$$\tau_{(perma\ i)} = \tau_i (a.F_{sc} + b) \quad (3)$$

Where  $a$  and  $b$  are tuneable dimensionless constants,  $F_{sc}$  is frost index, a value between 0 and 1, which is a measure of the balance between cold and warm days in a year, and is shown in eq. (4) where DDF are degree-days below 0°C and DDT are degree-days above 0°C in a year for daily average surface air temperature (Nelson and Outcalt 1987). DDF and DDT have units of °C.days/yr. Snow cover acts to insulate the ground against the coldest winter temperatures and reduces permafrost extent (Zhang 2005, Gouttevin et al. 2012). The subscript  $sc$  in eq. (3) and (4) indicate that these values are corrected for snow cover and represent the ground-snow interface conditions not the snow surface-air interface conditions.

$$F_{sc} = \frac{DDF_{sc}^{(1/2)}}{DDF_{sc}^{(1/2)} + DDT^{(1/2)}} \quad (4)$$

Including the frost-index as a multiplier (in eq. 3) for the permafrost soils carbon residence time was needed to allow the correct tuning of the model and allow for total land carbon stocks to be in agreement with data estimates. Therefore, the decomposition rates of soil carbon in permafrost affected cells are dependent on: mean annual temperature, (as with non-permafrost soils), the fractional cover of permafrost in the cell and the frost index (a measure of the severity of coldness in a year). This  $\tau_{perma\ i}$  (eq. 3) is only applied to the soils that are diagnosed as permafrost. The remainder of the carbon dynamics in land carbon pools was unaltered from the standard model.

### 2.3 1D model

We test a one dimensional model to compare the effect the different assumptions made for the model design. The total carbon stock in a grid cell using each method (sub-grid and re-mixing) was compared for equilibrium soil carbon content by running the 1D model for 100,000 simulation years. The carbon input from vegetation mortality is the same for both the



re-mixing and the sub-grid model, as is rainfall. The variables of permafrost fraction, mean annual air-surface interface temperature (MAT) and frost index are varied one at a time to compare the model outputs. The constants  $a$  and  $b$  for eq. (3) were set to 20 for  $\text{Soil}_{\text{fast}}$  and 2 for  $\text{Soil}_{\text{slow}}$  (so  $a$  and  $b$  have matching values) for the permafrost soils, and as the standard model for the non-permafrost soils. These values for  $a$  and  $b$  were chosen to compare the performance of the two methods, not for accurate soil carbon concentrations. They result in total carbon in the  $\text{Soil}_{\text{fast}}$  and the  $\text{Soil}_{\text{slow}}$  carbon pools being approximately equal to each other, which studies suggest is appropriate (Harden et al 2012, Zimov et al 2009).

Figure 3 shows the output for carbon content along a permafrost gradient, taking into account the relationship between permafrost-fraction, frost index and mean annual temperature. More detail on this figure is available in appendix A. The relationship between permafrost-fraction and frost index is defined as that determined in this study for the CLIMBER-2 model in section 3.2. As shown in eq. (1), NPP exerts a control on soil carbon content via input from plant material, although note that figure 3 shows model output for fixed NPP. For both approaches, carbon content increases non-linearly along the permafrost gradient (increasing permafrost fraction of the grid cell). The re-mixing model shows a stronger non-linear behaviour than the sub-grid model.

## 2.4 CLIMBER-2 modelled NPP

The comparisons of the sub-grid to re-mixing approaches shown in Figure 3 take no account of reductions in input to soils via NPP in colder climates. Figure 4 shows the CLIMBER-2 modelled NPP and the MODIS 2000-2005 mean NPP product (Zhao et al. 2011) for the present-day (PI, pre-industrial for CLIMBER output). The CLIMBER-2 vegetation model shows NPP patterns similar to the MODIS dataset. The boreal forest belt seen at around 60°N in the MODIS dataset is not clearly seen in the CLIMBER-2 model, mainly due to the large grid cell size. In Siberia and Alaska the NPP in CLIMBER-2 is not overestimated. The reduced NPP in the coldest regions would tend to reduce soil carbon accumulation via reduced input from plant mortality. Also shown in figure 4 are the upscaled data point plotted against CLIMBER-2 model output. The MODIS dataset represent the Earth system already subject to anthropogenic forcing, where the CLIMBER-2 model output represents the natural system only. However, the use of measurement based data to validate CLIMBER-2 NPP was preferred due to the quite large model spread seen in output for numerical global dynamic vegetation models of higher complexity than CLIMBER-2. The fact that MODIS is for the

1 present-day “perturbed” system (due to deforestation for example) may also explain some of  
2 the model-data mismatch, although we consider this is less significant for the permafrost zone  
3 low NPP soils which we are interested in. In order to test the applicability of the CLIMBER-2  
4 model for the glacial climate, a comparison of NPP for the LGM with a more complex model  
5 can be done (as measurement data is not available). Figure 5 shows LGM(eq) NPP for LPX  
6 (data courtesy M. Martin-Calvo, Prentice et al., 2011) and for CLIMBER-2 for an LGM  
7 climate. At LGM the NPP in Siberia and the coldest permafrost regions are non-zero in both  
8 models, and CLIMBER-2 follows the same general patterns as LPX predicts. CLIMBER-2  
9 shows slightly lower NPP in the southern parts of Russia, possibly similar to the boreal forest  
10 belt that is not well represented in the pre-industrial climate background NPP due to the large  
11 grid cell size. Again, the upscaled LPX data is shown plotted against CLIMBER-2 output,  
12 showing reasonable agreement on this scale. Overall at both periods, PI and LGM,  
13 CLIMBER-2 represents NPP reasonably well.

14 When the soil carbon content shown in figure 3 is adjusted to compensate for the reduction in  
15 NPP along a permafrost gradient and for the 0% permafrost socc data value (by multiplying  
16 relative value by 350), the resultant outputs are shown in figure 6 (more details are available  
17 in appendix A). Now, the re-mixing model shows a slight increase in total carbon along a  
18 permafrost gradient, where the sub-grid model shows a peak value at around 80% permafrost  
19 coverage. Figure 7 shows a comparison between these 1D model outputs and data for socc.  
20 The un-adjusted data is for the top 1m of soils, whereas model output represents the full soil  
21 column. As section 4.4, the model-data comparison is carried out by assuming that 40% of  
22 total soil carbon is located in the top 1m for permafrost soils (and is fully described in  
23 appendix A). From this comparison, the change in socc along a permafrost-gradient is  
24 relatively small, this is due to the combined effects of reducing soil decomposition rate and  
25 reducing NPP. Here, the re-mixing model represents quite well these changes. It may be  
26 possible to improve the performance of the sub-grid model by, for example, downscaling the  
27 climate variables also. However, this would represent a more significant change of the land  
28 biosphere model in CLIMBER-2, and increase the complexity and therefore the run speed of  
29 the model.

30 For the re-mixing model: at each time-step a proportion of carbon that is accumulated in the  
31 permafrost part is then sent back to decompose as standard soil. This occurs because the high  
32 carbon permafrost-soil carbon is mixed with the lower carbon standard soil in a grid cell at

1 each time step. This can be seen as similar to that which occurs in the active layer. The active  
2 layer is the top layer of the soil that thaws in warm months and freezes in cold months. In  
3 warm months the carbon in this thawed layer is available to be decomposed at “standard”  
4 soils rates, determined by local temperature. In the re-mixing model, the relative proportion of  
5 the permafrost soil carbon that is sent to decompose as standard soil carbon reduces along a  
6 permafrost gradient. This reduction can be seen as mimicking the characteristic of a reducing  
7 active layer thickness along a permafrost gradient, which is shown in figure 7 for active layer  
8 thickness data upscaled to the CLIMBER-2 grid size. Here active layer thickness mean is  
9 shown plotted against mean frost-index (and permafrost-fraction is directly calculated from  
10 frost-index in CLIMBER-2). It must be noted that on smaller spatial scales the relationship  
11 between the mean active layer thickness and the extent of permafrost in a location may be less  
12 clear. The local conditions determine both permafrost extent and active layer thickness. Our  
13 treatment for permafrost relies entirely on the relationships between climate characteristics  
14 and soil carbon contents on the CLIMBER-2 grid scale.

15

## 163 **CLIMBER-2 permafrost-carbon model**

17 We implemented eq. (3) into CLIMBER-2 using the re-mixing model. In order to study the  
18 effect of different carbon accumulation and release rates (the permafrost-carbon dynamics) in  
19 later modelling studies the soil carbon residence times can be tuned to distribute the carbon  
20 more into the Soil<sub>fast</sub> pool (making a quickly responding soil carbon pool) or more into the  
21 Soil<sub>slow</sub> pool (making a more slowly responding soil carbon pool). A total of 4 dynamic  
22 settings are retained for later coupled climate studies (described in section 3.5).

### 233.1 **Simulated climates to tune the permafrost-carbon model**

24 Three simulated climates were used to tune and validate the permafrost-carbon model: an  
25 LGM equilibrium climate: LGM(eq), a PI equilibrium climate: PI(eq), and a PI transient  
26 climate: PI(tr) obtained at the end of a transient deglaciation from the LGM climate. These  
27 three climates allow the total soil carbon to be tuned to the estimates of Ciais et al. (2012) for  
28 the LGM and PI climate conditions, these are described in table 1.

29

### 13.2 Calculating permafrost extent

In order to obtain a relationship between calculated frost-index and the permafrost-fraction of a grid cell, measurement and ground data for frost index and permafrost location were used. For present-day mean daily surface air temperatures, the freeze and thaw indices values on a 50.5° global grid were obtained from the National Snow and Ice Data Centre (NSIDC) database (Zhang et al. 1998). Using these values for freeze and thaw index a global frost index dataset on a 0.5° grid scale was created using eq. (4). The present-day estimates of land area that are underlain by permafrost are provided by Zhang et al. 2000, using the definition of zones: “continuous” as 90-100% underlain by permafrost, “discontinuous” as 50-90% underlain by permafrost, “sporadic” as 10-50% permafrost and “isolated” as less than 10%. Zhang et al. (2000) used these zonations to provide area estimates of the total land area underlain by permafrost. Summing the total land area that has a frost index higher than a particular value and comparing this to the Zhang et al. (2000) estimate can identify the appropriate boundary between permafrost and non-permafrost soils. Figure 8 shows the Zhang et al. (2000) permafrost areas for the high, medium and low ranges defined by the high, medium and low % estimates of permafrost zones marked as horizontal lines. The land area indicated by green squares is the total land surface in the northern hemisphere which has a frost-index value higher (where higher indicates a colder climate) than the cut-off value shown on the x-axis. Here the frost-index cut-off value of 0.57 shows good agreement with the medium (mean) estimate of the Zhang et al. (2000) total area of land underlain by permafrost.

### 223.3 Geographic permafrost distribution for the present-day

Figure 9 shows, coloured in blue, the land grid cells with a frost-index higher than 0.57 for 50.5° grid, with the north located at the centre of the map. Overlaid on this map area are the limits of the permafrost zones defined by the International Permafrost Association (IPA) (Jones et al. 2009). The frost-index value cut-off at 0.57 results in a southern limit of permafrost that represents approximately the middle of the discontinuous zone with some areas showing better agreement than others.

Figure 10 represents the upscaling of the 0.5° datasets for mean frost index and permafrost coverage to the CLIMBER-2 land grid scale. It shows the percentage of land in each CLIMBER-2 size grid cell defined as permafrost, (according to the 0.57 frost-index cut-off

1value shown in Fig. 8) plotted against the mean value of frost-index for the same grid cell.  
2Circled points in Figure 9 are where the grid cell has a large fraction of ocean (more than  
375%), and the milder ocean temperatures in winter reduce the mean frost-index value of the  
4whole grid cell. The dashed line shows a well-defined sigmoid function that relates frost  
5index to permafrost percentage of the land. We employ this relationship to predict permafrost  
6area in CLIMBER-2, as the frost-index can be calculated within the model from modelled  
7daily temperatures. Permafrost fraction is thus modelled as:

$$8 P_{landfraction} = A \left( 0.976 + \frac{\beta}{\sqrt{1+\beta^2}} \right) - 0.015 \quad (5)$$

9Where A and  $\beta$  are defined in table 2 and the model described in section 3.5. Frost index is  
10calculated from modelled daily surface temperatures and corrected for snow-cover. The snow  
11correction in our model is achieved using a simple linear correction of surface-air  
12temperature, using snow thickness to estimate the snow-ground interface temperature. This  
13correction is based on data from Taras et al (2003). The snow correction performs reasonably  
14well in CLIMBER-2 compared to measurement data from Morse and Burn (2010) and Zhang  
15(2005). This is because the large grid-cell size results in non-extreme snow depths and air  
16surface temperatures. The snow correction is described in Appendix B. Equation (6) shows  
17this linear model for snow correction, which is only applied for daily mean surface air  
18temperatures lower than -6°C. This snow-ground interface temperature is used to calculate the  
19freeze index ( $DDF_{sc}$ ) in eq. (4).

$$20 T_{g.i.} = T_{surf} - \frac{(T_{surf} + 6) \cdot SD}{100} \quad (6)$$

21Where  $T_{g.i.}$  is ground interface temperature (°C),  $T_{surf}$  is surface air temperature (°C) and SD is  
22snow depth (cm). Overall the effect of the snow correction within the model produced a  
23maximum decrease in permafrost area of 8% (compared to the uncorrected version) in the  
24most affected grid cell for the PI(eq) simulation and is therefore significant.

### 253.4 Permafrost extent tuning

26Using the snow-corrected frost-index value, four permafrost extent models representing the  
27range of values for permafrost area from Zhang et al. (2000) were determined. The model  
28settings are shown in table 2 and refer to A and  $\beta$  from eq. (5).  $P_{landfraction}$  is limited between 0  
29and 1, and the functions are plotted in Figure 10. These settings were identified by adjusting  
30the sigmoid function to obtain total permafrost area values at the PI(eq) simulation similar to

1the Zhang et al. (2000) areal estimates of permafrost and to maximise the difference in area  
2between the PI(eq) and LGM(eq) simulations permafrost extent. More complex models  
3underestimate permafrost extent at LGM (Levvasseur et al., 2011, Saito et al., 2013) quite  
4significantly and so by maximising the difference between PI and LGM permafrost, we  
5reduce the underestimate as far as possible for LGM permafrost extent.

### 63.5 Tuning the soil-carbon model

7Soil carbon content is controlled by the balance between soil carbon uptake and soil carbon  
8decomposition. There are four soil-carbon pools in CLIMBER-2; Soil<sub>fast</sub>: trees derived and  
9grass derived, Soil<sub>slow</sub>: trees derived and grass derived (eq.1). Soil<sub>fast</sub> have shorter carbon  
10residence times than Soil<sub>slow</sub>, so soil decays more quickly in Soil<sub>fast</sub> pools. The tunable  
11constants a and b (eq. 3) are independently applied for Soil<sub>fast</sub> and Soil<sub>slow</sub>, so carbon can be  
12placed relatively more in the Soil<sub>fast</sub> (Soil<sub>slow</sub>) pool as required in model tuning. Carbon is lost  
13from permafrost soils as the permafrost fraction of a grid cell reduces. If there is relatively  
14more (less) carbon in the Soil<sub>fast</sub> pool, this results in carbon that decays more quickly (more  
15slowly) when the permafrost thaws.

16At LGM, the area of permafrost on land was larger than today (Vandenberghe et al., 2012)  
17but not much information on soil carbon has been conserved, especially if it has long since  
18decayed as a result of permafrost degradation during the last termination. To constrain the  
19total carbon content in permafrost soils we use the estimates of Ciais et al. (2012), for total  
20land carbon these are  $3640 \pm 400 \text{ GtC}$  at LGM and  $3970 \pm 325 \text{ GtC}$  at PI, with a total change of  
21 $+330 \text{ GtC}$  between LGM and PI. The standard CLIMBER-2 model predicts total land carbon  
22stocks of  $1480 \text{ GtC}$  at LGM and  $2480 \text{ GtC}$  at PI, showing good agreement with the active-land-  
23carbon estimates of Ciais et al. (2012) (of  $1340 \pm 500 \text{ GtC}$  LGM and  $2370 \pm 125 \text{ GtC}$  PI). Any  
24'new' soil carbon is created via the permafrost-carbon mechanism and is assumed to be  
25equivalent to the inert land carbon pool estimates of Ciais et al. (2012). However, the dynamic  
26behaviour of permafrost-carbon in changing climates is not well constrained and it is for this  
27reason that a set of four dynamic settings were sought. Here the 'speed' of the dynamic setting  
28is determined by the ratio of total Soil<sub>fast</sub> pool to Soil<sub>slow</sub> pool carbon (fp/sp), with the "slow"  
29dynamic being fp/sp < 0.5, "medium" being fp/sp 0.5 to 1, "fast" being fp/sp 1 to 1.5 and  
30"extra-fast" being fp/sp > 1.5 for the PI-equilibrium simulation. The variables "a" and "b"  
31shown in eq. (3) were set and each setting used to run a PI(equilibrium), LGM(equilibrium)

1and PI(transient) simulation to identify the settings which resulted in total land carbon pools  
2in agreement with the Ciais et al. (2012) estimates.

3The LGM is conventionally defined as being the period around 21 kyrs BP, when large parts  
4of north America were underneath the Laurentide ice sheet. According to their time-to-  
5equilibrium (the slow carbon accumulation rate), soils in this location now free of ice may not  
6yet have reached equilibrium by the present day. Further than this, climate has changed  
7significantly since the LGM so permafrost soils anywhere may not be currently in equilibrium  
8(Rodionow et al. 2006), again due to its slow carbon accumulation rates. Due to this the PI(tr)  
9simulation model output for total land carbon was used to tune the total land carbon stocks, as  
10it includes a receding Laurentide ice sheet. At LGM, ice sheets were at maximum extent, so  
11the problem of land being newly exposed does not occur in the model. For this reason, the  
12LGM(eq) simulation is used to tune total land carbon for the LGM.

13Details of the tuning for total land carbon stocks are available in Appendix C. It was found  
14that only one permafrost area setting, the LOW-MEDIUM area, provided an acceptable range  
15of dynamic settings, as defined by the ratio of fast to slow soil carbon. The four selected  
16dynamics settings are shown in more detail in Figure 12: for total land carbon stock,  
17atmospheric CO<sub>2</sub> and ratio of fast to slow soil-carbon pool. The a and b values for these  
18settings are shown in table 3.

19To evaluate the effect of the different dynamic settings we ran an equilibrium PI simulation  
20for all four selected settings for 40kyrs, followed by a permafrost switch-off for a further 10k  
21yrs. Figure 12 shows the global total land carbon stocks for this experiment. The period  
22between 0-40k simulation years demonstrate the transient effects of the slow accumulation  
23rates in permafrost soils. Depending on the dynamic setting, the total land carbon takes more  
24than 40k years to fully equilibrate in PI climate conditions. On permafrost switch-off, from  
2540k sim years, the soil-carbon previously held in permafrost soils is quickly released to the  
26atmosphere, at a rate dependent upon the dynamic setting. The xfast setting releasing all  
27excess carbon within hundreds of years and the slow setting around 8000 years after total  
28permafrost disappearance. Currently, the most appropriate carbon dynamic setting is  
29unconstrained by measurement data. It is for this reason that the permafrost-carbon dynamics  
30settings cover a large range. They are intended to be used in transient model simulations to  
31better constrain permafrost-carbon dynamics in changing climate. . It should be noted that the  
32PI(eq) simulation was not used to tune the model, i.e. was not used to compare model output

1to Ciaia et al 2012 PI total land carbon stocks. Figure 13 demonstrates only the range of  
2dynamic response for all four settings. This PI(eq) simulation also demonstrates the difference  
3between transient versus equilibrium PI simulations. The slow dynamic equilibrates (after  
4more than 40k years) at far higher total carbon stocks than the xfast dynamic, but for the PI(tr)  
5simulation these two settings show very similar total land carbon stocks (we selected them for  
6this behaviour).

7

## 84 Model Performance

9Hereafter, the name “CLIMBER-2P” denotes the model in which the permafrost-carbon  
10mechanism operates fully coupled within the dynamic vegetation model.

### 114.1 Permafrost areal coverage and spatial distribution

12Figure 14a shows the spatial pattern of permafrost as predicted in CLIMBER-2P with the  
13snow correction included for the LOW-MEDIUM area setting. The modelled PI(tr)  
14permafrost extent fairly well estimates the location of the present-day southern boundary of  
15the discontinuous permafrost zone (Jones et al. 2009), with overestimate of permafrost extent  
16in the western Siberian grid cell, and underestimate over the Himalayan plateau. Total  
17permafrost area extent is shown in table 4.

18Comparing this to performance of other models (Levvasseur et al. 2011), the PI(eq) total  
19permafrost area is closer to Zhang et al. (2000) estimates, but it must be kept in mind that for  
20CLIMBER-2P the area was tuned to be in agreement with mean estimate from Zhang et al.  
21(2000). The PI(tr) total permafrost area is higher by around  $4 \times 10^6 \text{ km}^2$  compared to the PI(eq).  
22This is due to the North Pacific region being colder in PI(tr) than that of the PI(eq) simulation,  
23and may be related to the land run-off, which is kept at LGM settings for the transient  
24simulations. For LGM period, the best PMIP2 model in the Levvasseur study (interpolated  
25case) underestimated total permafrost area by 22% with respect to data estimates (of  $33.8 \times$   
26 $10^6 \text{ km}^2$ ), and 'worst' model by 53%, with an all-model-median value of 47% underestimate.  
27The LOW-MEDIUM CLIMBER-2P setting gives an LGM total permafrost area  
28underestimate of around 40%, slightly better than the median for PMIP2 models' permafrost  
29area.



Figure 14b shows the LGM CLIMBER-2P permafrost extent with the reconstructed continuous and discontinuous southern boundaries (Vandenberghe et al., 2012, French and Millar, 2013) overlaid. In the LGM simulation for CLIMBER-2P, coastlines do not change so the Siberian Shelf and other exposed coastlines in the northern polar region are not included in the CLIMBER-2P permafrost area estimate. These coastal shelves cover an estimated area of 5 to 7 x 10<sup>6</sup> km<sup>2</sup>. Another area which is not diagnosed as permafrost in CLIMBER-2P is the Tibetan plateau, which would be an additional estimated 6 x 10<sup>6</sup> km<sup>2</sup>. If these two regions were added (totalling around 12 x 10<sup>6</sup> km<sup>2</sup>) to the LGM area estimate it would bring the modelled permafrost area (then totalling around 33 x 10<sup>6</sup> km<sup>2</sup>) much closer to the data estimate as reported in the Levvasseur et al. (2011) study. The permafrost extent model is dependent upon the CLIMBER-2P modelled climate. The very large grid cell size of CLIMBER-2P means that modelled mountainous regions such as the Tibetan plateau are problematic, resulting in a possible too-warm climate (compared to the real-world) in this region.

#### 14.2 Soil carbon dynamics

Accumulation rates show general agreement with the Zimov et al. (2009) model and the Wania et al. (2009b) (LPJ) model, although the fast and xfast dynamic settings accumulate carbon faster than these comparison models. Figure 15 shows output for all permafrost dynamic for the PI (equilibrium) spin-up. The north west Siberia site can be compared to the Ayach-Yakha location from the Wania et al. (2009b) and to the extra-cold conditions from Zimov et al. (2009). The Ayach-Yakha modelled site in Wania et al. (2009b) has a time to equilibrium of greater than 80 kyr and soil carbon content of greater than 200 kg/m<sup>2</sup>, the Zimov model predicts that 200 kg/m<sup>2</sup> soil carbon content can be reached within 10k years in the top layer of the soil and 150 kg/m<sup>2</sup> for the full soil column taking longer than ~50 kyr to reach equilibrium. The N. Canada (Fig 15) location takes a longer time to reach equilibrium than soils in the N.W. Siberia grid cell. NPP in the N. Canada grid cell is less than one third of that for the N.W. Siberia grid cell. Due to the lower soil carbon input there is a lower range in the output between the difference carbon dynamic settings for the N. Canada grid cell. Northern Canada was underneath the Laurentide ice sheet at LGM. Since the demise of the Laurentide ice sheet around 13 kyr ago (Denton et al., 2010) there has not been enough time for these soils to equilibrate, which takes longer than 40k years according to our model. As well as this, this region has very high water contents (and islands) which are not represented in CLIMBER-2P which may modify soil carbon concentrations. Although we do not account for

1 water content, we can take account of the demise of the laurentide ice sheet and the time that  
2 these soils have had to accumulate carbon. The PI climate condition and soil carbon content  
3 that we applied to tune and validate the model is the PI(tr), the transient simulation, which  
4 includes ice sheet evolution.

### 54.3 Soil carbon stocks

6 The total land carbon stocks were tuned using data from Ciais et al. (2012). An assumption  
7 made in this study is that all 'extra' soil carbon, relative to the standard model, in the Arctic  
8 region is located in permafrost soils and only by the mechanism of increased soil carbon  
9 residence time in frozen soils. Table 5 shows the Ciais et al. (2012) land carbon pools values  
10 that have been used to tune this model. The standard model total land carbon (tlc) are similar  
11 to the active land carbon stocks, with PI tlc at 2199GtC and LGM tlc at 1480GtC (shown in  
12 table 7).

13 The soil types that are found in the continuous and discontinuous permafrost zone are the  
14 Cryosols (circumpolar atlas) or Gelisols (Soil taxonomy). Within this group are further  
15 subgroups; Turbels which are subject to cryoturbation and characterise the continuous  
16 permafrost zone, Orthels which are less affected by cryoturbation and are related to  
17 discontinuous permafrost and Histels which relate to peat growth (histosols) and have  
18 permafrost at less than 2m depth. Histels are not directly represented in the simplified model,  
19 as they are dominated by peat growth (Sphagnum), a distinct PFT not represented in  
20 CLIMBER-2P.

21 The Tarnocai et al. (2009) soil organic carbon content (socc) estimates for the present-day for  
22 relevant soils are shown in table 6. Summing "All soils" with loess soils and Deltaic deposits  
23 gives the 1672GtC estimated total socc for the permafrost region. The extra land carbon  
24 stocks created in our model in permafrost soils range between 1620GtC to 2226GtC (table 8)  
25 compared to Tarnocai et al. at 1672GtC and 1600+-300GtC in the Ciais et al estimate for inert  
26 land carbon for the present day. For the LGM climate, the model shows a range of 1987GtC  
27 to 2117GtC for extra soil carbon compared to the Ciais estimate of 2300+-300GtC for inert  
28 land carbon. The "medium" dynamic setting shows total land carbon stocks in the present-day  
29 outside the range estimated by Ciais et al. However, during tuning (see Appendix C) this  
30 overestimate could not be improved upon.

#### 14.4 Soil carbon contents validation

The carbon content of Orthels and Turbels decreases with depth, but high carbon contents are still found at depths of 3m and more (Tarnocai et al., 2009). For Orthels (with alluvium) around 80% of their carbon content was found in the top 200cm and for Turbels 38% of carbon content was found in the top 100cm. Based on these values, to compare the CLIMBER-2P output with ground spatial data, it is assumed that 40% of the modelled total soil-column carbon is located in the top 100cm for all permafrost affected soils.

Soil carbon data from Hugelius et al. (2013) was used to compare against the CLIMBER-2P output. The Orthels and Turbels dominate the continuous and coldest permafrost areas, with Histels and other soils becoming more dominant towards the southern parts of the permafrost region. As no peatlands or wetlands are represented in our simplified model, only Orthel and Turbel soils were used as comparison points for soil organic carbon content (socc). Socc data from Hugelius et al. (2013), for grid cells with 50% or more Orthel and Turbel soils, was upscaled to the CLIMBER-2P grid. These mean socc data values for the top 1m of soil were plotted against CLIMBER-2P model output for matching grid cells, this is shown in Figure 16. Also shown in Fig. 16 is the standard model output, which has no permafrost mechanism. Two grid cells show very much higher socc than data suggests, with around a three fold overestimate and are located in Siberia. All other grid cells are within a range of  $\pm 80\%$  heavily dependent on the soil carbon dynamic setting. The standard model shows progressively worse performance as mean socc increases in the data. The permafrost model shows an increasing socc trend more similar to data. Comparing the spatial location of socc to data can be done using Fig. 17. The two grid cells with very high socc compared to data are central and eastern Siberia. These grid cells are both 100% permafrost and have had a total of 101k years (80k for LGM(eq) plus 21k to PI(tr)) years to accumulate carbon. This is in contrast to the North American continent grid cells which were underneath the ice sheet until the deglaciation, so have had less time to accumulate carbon.

The assumption that all permafrost region soil-carbon acts as Turbels and Orthels has an impact on the physical location of the socc with respect to data. Turbels and Orthels are located in the northern parts of the permafrost zone with Histels and other soils becoming more dominant to the south. Compared to socc in ground data (Fig. 17), a northern bias in socc is seen in model output, as expected. Histels (peatland soils) and other soil types of the permafrost zone, with an estimated 390GtC (table 6) are not represented in our model. If these

1 were modelled they should increase socc in model output in the more southern part of the  
2 permafrost region, and parts of Canada. Large river deltas, which contain deltaic deposits of  
3 241 GtC (Tarnocai et al. 2009) are also not represented in our model. One example of this is  
4 the Ob river and Gulf of Ob, located in western Siberia which, combined with dominance of  
5 Histels in this region (Hugelius et al. 2013), cause a high socc in data. The model does not  
6 represent well the boreal forest belt (see Fig. 4) which is also located in the southern region of  
7 the permafrost zone. This results in carbon input to soils in this region being underestimated  
8 in our model.

9 Figure 18 shows the model outputs for the LGM climate. No soil carbon is present underneath  
10 ice sheets and the highest carbon concentrations are seen in present day south-eastern Russia  
11 and Mongolia, with quite high soil carbon concentrations in present day northern Europe and  
12 north-western Russia. Comparing this output to the permafrost extent model (Fig. 14), the  
13 socc is likely located too far north for the same reasons as the PI(tr) socc but also because  
14 permafrost extent is underestimated for the LGM(eq) climate. The northern China region,  
15 according to data, was continuous permafrost at LGM as was the south west Russia region.  
16 These regions would have higher socc in model output if the modelled permafrost area was  
17 closer to data estimates. The same would be true of the Siberian shelf. This means that the  
18 extra soil carbon tuned to the Ciais et al. (2012) estimate (table 5) is concentrated in a central  
19 band in Eurasia more so than the model would predict if permafrost extent was more like the  
20 data estimate for LGM.

21

## 22 **5 Model applications and limitations**

### 23 **5.1 Applications**

24 The simplified permafrost mechanism is intended to be used for the study of carbon-cycle  
25 dynamics on timescales of centuries/millennia and longer. It represents an improvement on  
26 the previous terrestrial carbon cycle model in CLIMBER-2 which did not include any effects  
27 of frozen soils. It is not intended for the study of carbon cycle dynamics on scales shorter than  
28 centuries due to the simplifications made and many processes not accounted for in the  
29 simplified model. The permafrost-carbon mechanism is dependent upon the relationship  
30 between climate, soil carbon content and active layer thickness on the CLIMBER-2 grid scale.  
31 To apply this parametrisation of permafrost-carbon to other grid scales, the relationship of

1active layer thickness and climate variables would need to be re-assessed. The relationship  
2between permafrost fraction of a grid cell and soil organic carbon content is non-linear. The  
3values for “a” and “b” would need to be re-tuned in order to output total land carbon stocks in  
4agreement with Ciais et al 2012 for grid scales different to the CLIMBER-2 grid.

5The permafrost-carbon mechanism is fully dynamic and responds to changes in: insolation  
6(orbit), atmospheric CO<sub>2</sub> (via changes in NPP and climate), land area in response to coverage  
7by ice sheets extending or contracting. This could not be easily achieved if a box model  
8representation of permafrost-carbon was applied as the model response to the drivers (orbit,  
9CO<sub>2</sub> and ice sheet) are dependent upon spatial location.

## 105.2 Simplifications and limitations

11The permafrost model does not make any changes to soil carbon based on hydrology or ice  
12contents. Precipitation only affects vegetation growth, not soil formation.

13No account is taken of the effect of peatland soils in permafrost regions as the PFT for  
14Sphagnum species, which accounts for most of peat soil vegetation cover, is not included in  
15the model. The effect of frozen ground inhibiting root growth (to depth) is not accounted for,  
16which may have an impact on the GPP and soil formation in very cold regions.

17During glacial climates, no extra land is exposed as sea-level drops in the CLIMBER-2P  
18model, all the carbon used to tune the carbon dynamics for LGM period is located on land that  
19is presently above sea-level.

20Wetlands and river deltas increase the spatial spread of the soil carbon in the real world, and  
21these are not represented in CLIMBER-2P. Therefore, it is also not intended that the spatial  
22location of the highest soil carbon concentrations should be used as a very good indicator of  
23the real world case.

24Slow accumulation rates in permafrost soils result in the characteristic that in the real world  
25during thaw (or deepening of the active layer) the youngest soils would decompose first. In  
26CLIMBER-2P all soil is mixed, so the age of carbon down the soil column cannot be  
27represented. This age of the soils is important for the correct modelling of <sup>14</sup>C then seen in the  
28atmosphere. The model has no soil 'depth' (only a carbon pool) so <sup>14</sup>C cannot be used as a  
29useful tracer as part of CLIMBER-2P in its current configuration. The CLIMBER-2P model

1does have a  $^{13}\text{C}$  tracer within the carbon cycle which is intended to be used in conjunction  
2with the permafrost model to constrain carbon cycle dynamics.

3The possible impact of high dust concentrations on soil formation during glacial climates is  
4not accounted for in the model. Loess soils, those created by wind-blown dust or alluvial  
5soils, are not represented. For our study it is assumed that the ratio of loess to non-loess soils  
6is the same in the present day as it was during glacial climates. This is not the case in the real  
7world, where high dust concentrations in the dry atmosphere increased loess deposition at  
8LGM (Frechen 2011). However, the LGM climate is only representative of the coldest and  
9driest period of the last glacial. Evidence suggests that soils were productive in cold  
10conditions in the permafrost region of the last glacial period with loess accumulation only  
11more widely significant towards the harsh conditions of the LGM (Elias and Crocker., 2008,  
12Chlachula and Little., 2009, Antoine et al., 2013, Willerslev et al., 2014).

13No changes were made to the vegetation model or to controls on soil input which are only  
14dependent upon temperature and NPP, the Mammoth-Steppe biome is not explicitly modelled  
15(Zimov et al. 2012).

16Underneath ice-sheets soil carbon is zero, as an ice sheet extends over a location with soil  
17carbon (and vegetation), that carbon is released directly into the atmosphere. As an ice sheet  
18retreats and exposes ground, the vegetation (and soil) can start to grow again. So, our model  
19does not account for any carbon that may have been buried underneath ice sheets (Wadham et  
20al., 2012).

21

## 226 **Conclusions/summary**

23This permafrost-carbon model is a simplified representation of the general effect of frozen  
24ground on soil carbon decomposition. In the presence of frozen ground the soil carbon decays  
25more slowly. The method by which permafrost is diagnosed relies only on the balance  
26between warm (above  $0^{\circ}\text{C}$ ) and cold (below  $0^{\circ}\text{C}$ ) days, which removes the problem of  
27compounding errors in thermal diffusion calculations (for example). As such, the permafrost-  
28carbon model would perform just as well in distant past climates as it does in pre-industrial  
29climate. In order to account for uncertainties in carbon accumulation and release rates in  
30frozen (and thawing) soils, a range of dynamic settings are retained which agree with total  
31land carbon estimates of Ciais et al. (2012). Due to the slow accumulation in permafrost soils,

1soil carbon has a long time to equilibrium and therefore the present-day climate must be  
2treated as a transient state, not as an equilibrium state. We showed the model performs  
3reasonably well at pre-industrial present-day conditions. The permafrost-carbon model creates  
4a mechanism which slowly accumulates soil carbon in cooling or cold climates and quickly  
5releases this high soil carbon in warming climates, caused either by changes in insolation  
6patterns or by global increases in temperature and climatic changes due to greenhouse gas  
7feedbacks and ocean circulation changes. It can thus be used to quantitatively evaluate the  
8role of permafrost dynamics on the carbon build-up and release associated with this specific  
9physical environment, over supra-centennial to glacial-interglacial timescales.

10

## 11**Appendix A: 1D models**

12Figure A1 shows the results of sensitivity experiments comparing these two approaches for  
13one CLIMBER-2 land grid cell. Baseline settings of permafrost fraction = 0.6, Frost index =  
140.6, mean annual air temperature = -10°C have a relative soil carbon concentration of 1. The  
15sub-grid method outputs a linear-type relationship between permafrost fraction and soil  
16carbon stored. The re-mixing model outputs lower soil carbon concentration for lower  
17fractional permafrost coverage rising quickly when permafrost fraction approaches 1. For the  
18air temperature as variable, the two approaches show a similar response. For higher frost  
19index the soil carbon concentration increases, with the sub-grid method showing slightly more  
20sensitivity than the re-mixing model.

21The variables of permafrost fraction, frost index and mean annual temperature are inter-  
22related, and co-vary. The relationships between these variable are shown in figure A2a. For  
23permafrost-fraction to frost-index, the relationship is defined as that determined in the main  
24text for the CLIMBER-2 grid scale in section 3.2.

25When including the effect of NPP, the equilibrium total carbon contents are scaled according  
26to the relationship between NPP and permafrost fraction. Figure A2b shows MODIS data for  
27NPP plotted against frost index (calculated from data from Zhang et al 1998 for freeze (DDF)  
28and thaw (DDT) values to be used in eq. (4) from the main text). This data is upscaled to the  
29CLIMBER-2 grid and plotted against permafrost-fraction (calculated from the frost-index  
30value). The values are only for NPP in the high northern latitudes.

31

To compare model output to data, it is assumed that 40% of total soil column carbon is located in the top 1m for permafrost soils (Tarnocai et al 2009). To convert socc (top 1m) to full column, the socc data is multiplied by (2.5\*permafrost\_fraction). This soil carbon content is plotted against calculated permafrost fraction, that is, using the model from section 3.2 to get permafrost-fraction from frost-index data. This socc data is then binned into 0.1 increases in permafrost fraction and the mean value is shown with  $\pm 1\sigma$  in figure 7 (main text).

7

## 8Appendix B: Snow correction

### 9B.1 Linear model

In more complex physical models, snow correction of ground temperature is achieved by modelling the thermal diffusion characteristics of the snow cover; a function of snow depth and snow type (for example snow density). A thermal diffusion model is used to make an estimate of the snow-ground interface temperature using the surface air temperature, the thermal gradient is also dependent upon the initial snow-ground interface temperature. Within the CLIMBER-2 model, snow is already modelled (Petoukhov et al., 2000) as it has a significant effect on overall climate (Vavrus, 2007). Snow depth in CLIMBER-2 is available as well as snow fraction per cell, but snow type and snow density is not individually modelled. Attempting to model the thermal diffusion in the snow does not make sense for CLIMBER-2, as with permafrost location. Rather the approach is to use measurement data to create a general relationship between air temperature and snow-ground interface temperature based only on the snow depth.

The snow correction linear model is based on data from Taras et al. (2002) giving a correction for snow-ground interface temperature from snow depth and air temperature. Figure B1a shows the data from Taras et al. (2002) and the linear regressions (labelled as A, B and C) of this data re-plotted per snow depth (Fig. B1b). Equation (B.1) shows this linear model for snow correction, which is only applied for surface air temperatures lower than  $-6^{\circ}\text{C}$ . This snow-ground interface temperature is used to calculate the freeze index ( $\text{DDF}_{\text{sc}}$ ) in eq. (4) in the main text.

$$29 \quad T_{g.i.} = T_{surf} - \frac{(T_{surf} + 6) \cdot SD}{100} \quad (\text{B.1})$$

Where  $T_{g.i.}$  is ground interface temperature ( $^{\circ}\text{C}$ ),  $T_{surf}$  is surface air temperature ( $^{\circ}\text{C}$ ) and SD is snow depth (cm)



## 2B.2 Snow correction validation

3This simple snow-correction was tested against data from Morse and Burn (2010). Figure B2  
4shows the error made by the linear model when used to predict the snow-ground interface  
5temperature (or snow depth temperature) from Morse and Burn measurement data. In the  
6more extreme conditions, the error of the linear model is far higher, for example in deep snow  
7and cold temperatures. Figure B3 shows the outputs from CLIMBER-2 for snow depths  
8plotted against surface air temperatures for the PI(eq) pre-industrial climate (green circles)  
9and LGM(eq) glacial climate (blue squares) for all grid cells. The large CLIMBER-2 grid size  
10means that extreme conditions are not present in the model output. Comparing Figures B2 and  
11B3 shows that the linear correction can provide an estimated confidence within  $-8^{\circ}\text{C}$  for the  
12deepest snow cover and highest temperatures of CLIMBER-2P data output, and within  $+2^{\circ}\text{C}$   
13for the majority of CLIMBER-2P data outputs. A similar performance is found when  
14comparing to snow thickness and snow-ground interface temperatures from Zhang (2005) for  
15a site in Zyryanka, Russia. The most extreme temperatures and snow conditions produce a  
16larger error from the linear model, but the intermediate conditions, those seen in CLIMBER-  
172P data points, agree better with the data. Overall the effect of the snow correction within the  
18model produced a maximum decrease in permafrost area of 8% (compared to the uncorrected  
19version) in the most affected grid cell for the PI(eq) simulation and is therefore significant.

20

## 21Appendix C: Tuning for total land carbon at the LGM and PI

22Table C1 shows all the settings for 'a' and 'b' per soil pool (eq. (3), main text) that were tested  
23to obtain total soil carbon contents for the LGM and the PI simulations. Figure C1 shows the  
24modelled total land carbon (GtC) for all simulations sorted by permafrost area function. Green  
25dashed lines on the LOW-MEDIUM area setting indicate the dynamic settings chosen to  
26represent the "slow", "medium", "fast" and "extra-fast" permafrost-carbon dynamic settings.  
27The total land carbon content is clearly very sensitive to permafrost area, and despite many  
28simulation tunings only the LOW-MEDIUM area setting provided a good enough range of  
29dynamics that could be used to later investigate the permafrost-carbon dynamics. Within the  
30settings chosen, the "medium" dynamic setting overestimated the present-day total land  
31carbon estimate from Ciais et al 2012, but further tuning experiments did not improve this  
32over-estimate.

## 2**Acknowledgements**

3The research leading to these results has received funding from the European Community's  
4Seventh Framework Programme (FP7 2007-2013) under Grant 238366 (GREENCYCLES II)  
5and under grant GA282700 (PAGE21, 2011-2015). D.M. Roche is supported by INSU-CNRS  
6and by NWO under project no. 864.09.013.

## 1References

- 2Aleksandrova, L.N.: Processes of humus formation in soil, Proceedings of Leningrad  
3Agricultural Institute. Leningrad. 142, 26-82, 1970. In Russian
- 4Alexeev V.A., Nicolsky D.J., Romanovsky V.E., Lawrence D.M.: An evaluation of deep soil  
5configurations in the CLM3 for improved representation of permafrost. Geophysical Research  
6Letters, 34, L09502, doi:10.1029/2007GL029536, 2007.
- 7Antoine, P., Rousseau, D. D., Degeai, J. P., Moine, O., Lagroix, F., Fuchs, M., ... & Lisá, L.:  
8High-resolution record of the environmental response to climatic variations during the Last  
9Interglacial–Glacial cycle in Central Europe: the loess-palaeosol sequence of Dolní Věstonice  
10(Czech Republic). Quaternary Science Reviews, 67, 17-38, 2013.
- 11Bouttes, N., Roche D.M., Paillard D.: Impact of strong deep ocean stratification on the glacial  
12carbon cycle. Paleoceanography. 24. PA3202. Doi: 10.1029/2008PA001707, 2009.
- 13Bouttes N., Paillard D., Roche D.M., Brovkin V., Bopp L.: Last Glacial Maximum CO<sub>2</sub> and  
14δ<sup>13</sup>C successfully reconciled. Geophysical Research Letters. 38, L02705,  
15doi:10.1029/2010GLO44499, 2011.
- 16Bouttes, N., Paillard, D., Roche, D.M., Waelbroeck, C., Kageyama, M., Laurantou, A.,  
17Michel, E., Bopp, L. and Siddall, M.: Impact of oceanic processes on the carbon cycle during  
18the last termination. Climate of the Past. 8, 1, 2012.
- 19Brovkin V., Ganopolski A., Archer D., Rahmstorf S.: Lowering of glacial atmospheric CO<sub>2</sub> in  
20response to changes in oceanic circulation and marine biogeochemistry. Paleoceanography.  
2122. PA4202. Doi: 10.1029/2006PA001380, 2007.
- 22Brovkin V., Ganopolski A., Svirezhev Y.: A continuous climate-vegetation classification for  
23use in climate-biosphere studies. Ecological Modelling. 101: 251-261, 1997
- 24Brown, J., K. Hinkel, and F. Nelson (comp.). Circumpolar Active Layer Monitoring (CALM)  
25Program Network. Boulder, Colorado USA: National Snow and Ice Data Center. 2003
- 26Chlachula, J., & Little, E.: A high-resolution Late Quaternary climatostratigraphic record  
27from Iskitim, Priobie Loess Plateau, SW Siberia. Quaternary International, 240(1), 139-149,  
282011.

- 1Ciais P., Tagliabue A., Cuntz M., Bopp L., Scholze M., Hoffman G., Laurantou A., Harrison  
2SP., Prentice IC., Kelley DI., Koven C., Piao SL.: Large inert carbon pool in the terrestrial  
3biosphere during the Last Glacial Maximum. *Nature Geoscience*. 5: 74. doi:  
410.1038/NGEO1324, 2012.
- 5Collins, M., R. Knutti, J. Arblaster, J.-L. Dufresne, T. Fichefet, P. Friedlingstein, X. Gao,  
6W.J. Gutowski, T. Johns, G. Krinner, M. Shongwe, C. Tebaldi, A.J. Weaver and M. Wehner,  
72013: Long-term Climate Change: Projections, Commitments and Irreversibility. In: *Climate*  
8*Change 2013: The Physical Science Basis. Contribution of Working Group I to the Fifth*  
9*Assessment Report of the Intergovernmental Panel on Climate Change* [Stocker, T.F., D. Qin,  
10G.-K. Plattner, M. Tignor, S.K. Allen, J. Boschung, A. Nauels, Y. Xia, V. Bex and P.M.  
11Midgley (eds.)]. Cambridge University Press, Cambridge, United Kingdom and New York,  
12NY, USA, 2013.
- 13Dankers R., Burke EJ., Price J.: Simulation of permafrost and seasonal thaw depth in the  
14JULES land surface scheme. *The Cryosphere*. 5:773-790. doi: 10.5194/tc-5-773-2011, 2011.
- 15Denton, G. H., Anderson, R. F., Toggweiler, J. R., Edwards, R. L., Schaefer, J. M., &  
16Putnam, A. E.: The last glacial termination. *Science*, 328(5986), 1652-1656, 2010.
- 17Ekici, A., Beer, C., Hagemann, S., Boike, J., Langer, M., and Hauck, C.: Simulating high-  
18latitude permafrost regions by the JSBACH terrestrial ecosystem model, *Geosci. Model Dev.*,  
197, 631-647, doi:10.5194/gmd-7-631-2014, 2014.
- 20Elias, S. A., & Crocker, B.: The Bering Land Bridge: a moisture barrier to the dispersal of  
21steppe–tundra biota?. *Quaternary Science Reviews*, 27(27), 2473-2483, 2008.
- 22Fischer, H., Schmitt, J., Lüthi, D., Stocker, T. F., Tschumi, T., Parekh, P., ... & Wolff, E.: The  
23role of Southern Ocean processes in orbital and millennial CO<sub>2</sub> variations – A synthesis.  
24*Quaternary Science Reviews*, 29(1), 193-205, 2010.
- 25Frechen, M.: Loess in Eurasia. *Quaternary International*, 234(1), 1-3, 2011.
- 26French, H.M. and Millar, SWS.: Permafrost at the time of the Last Glacial Maximum (LGM)  
27in North America. *Boreas*, doi:10.1111/bor.12036, 2013.
- 28Ganopolski A., Petoukhov V., Rahmstorf S., Brovkin V., Claussen M., Eliseev A., Kubatzki  
29C.: CLIMBER-2: a climate system model of intermediate complexity. Part II: model  
30sensitivity. *Climate Dynamics*. 17: 735-751, 2001.

1Gouttevin, I., Menegoz, M., Dominé, F., Krinner, G., Koven, C., Ciais, P., Tarnocai, C., and  
2Boike, J.: How the insulating properties of snow affect soil carbon distribution in the  
3continental pan-Arctic area. *Journal of Geophysical Research: Biogeosciences* (2005–2012),  
4117(G2), 2012.

5Harden JW, Koven CD., Ping CL, Hugelius G., McGuire AD., Cammill P., Jorgenson T.,  
6Kuhry P., Michaelson GJ., O'Donnell JA., Schuur EAG., Tarnocai C., Johnson K., Grosse G.:  
7Field information links permafrost carbon to physical vulnerabilities of thawing. *Geophysical*  
8*Research Letters*. 39. L15704. Doi:10.1029/2012GL051958, 2012.

9Hugelius, G., Tarnocai, C., Broll, G., Canadell, J. G., Kuhry, P., and Swanson, D. K.: The  
10Northern Circumpolar Soil Carbon Database: spatially distributed datasets of soil coverage  
11and soil carbon storage in the northern permafrost regions, *Earth System Science Data*, 5, 3-  
1213, doi:10.5194/essd-5-3-2013, 2013.

13Jones, A., V. Stolbovoy, C. Tarnocai, G. Broll, O. Spaargaren and L. Montanarella (eds.):  
14Soil Atlas of the Northern Circumpolar Region. European Commission, Office for Official  
15Publications of the European Communities, Luxembourg. 142 pp. 2009.

16Koven C., Friedlingstein P., Ciais P., Khvorostyanov D., Krinner G., Tarnocai C.: On the  
17formation of high-latitude soil carbon stocks: Effects of cryoturbation and insulation by  
18organic matter in a land surface model. *Geophysical Research Letters*. 36. L21501. Doi:  
1910.1029/2009GL040150, 2009.

20Koven, C. D., Riley, W. J., & Stern, A.: Analysis of permafrost thermal dynamics and  
21response to climate change in the CMIP5 Earth System Models. *Journal of Climate*, 26(6),  
221877-1900, 2013.

23Levavasseur G., Vrac M., Roche DM., Paillard D., Martin A., Vandenberghe J.: Present and  
24LGM permafrost from climate simulations: contribution of statistical downscaling. *Climate of*  
25*the Past*. 7: 1225-1246. doi: 10.5194/cp-7-1225-2011, 2011.

26Lourantou A., Lavric J.V., Kohler P., Barnola JM., Paillard D., Michel E., Raynaud D.,  
27Chappelaz J.: Constraint of the CO<sub>2</sub> rise by new atmospheric carbon isotopic measurements  
28during the last deglaciation. *Global Biogeochemical Cycles*, 24, BG2015,  
29doi:10.1029/2009GB003545. 2010,

30Maslin, M. A., & Thomas, E.: Balancing the deglacial global carbon budget: the hydrate  
31factor. *Quaternary Science Reviews*, 22(15), 1729-1736, 2003.

1 Monnin, E., Indermühle, A., Dällenbach, A., Flückiger, J., Stauffer, B., Stocker, T. F.,  
2 Raynaud, D., and Barnola, J. M.: Atmospheric CO<sub>2</sub> concentrations over the last glacial  
3 termination. *Science*, 291(5501), 112-114, 2001.

4 Morse PD., Burn CR.: Ground temperature variation with snow, Kendall Island Bird  
5 Sanctuary, outer Mackenzie Delta, Northwest Territories. GEO2010, 2010.

6 Nelson FE., Outcalt SI.: A computational method for prediction and regionalization of  
7 permafrost. *Arctic and Alpine Research*. 19(3): 279-288, 1987.

8 Peltier, W. R.: Global glacial isostasy and the surface of the ice-age Earth: The ICE-5G  
9 (VM2) Model and GRACE, *Ann. Rev. Earth Planet. Sci.*, 32, 111–149,  
10 doi:10.1146/annurev.earth.32.082503.144359, 2004.

11 Petoukhov V., Ganopolski A., Brovkin V., Claussen M., Eliseev A., Kubatzki C., Rahmstorf  
12 S.: CLIMBER-2: a climate system model of intermediate complexity. Part 1: model  
13 description and performance for present climate. *Climate Dynamics*. 16:1-17, 2000.

14 Prentice, I. C., Harrison, S. P., and Bartlein, P. J.: Global vegetation and terrestrial carbon  
15 cycle changes after the last ice age. *New Phytologist*. 189(4), 988-998, 2011.

16 Riseborough D., Shiklomanov N., Etzelmüller B., Gruber S., Marchenko S.: Recent advances  
17 in permafrost modelling. *Permafrost and Periglacial Processes*. 19: 137-156, 2008.

18 Saito, K., T. Sueyoshi, S. Marchenko, V. Romanovsky, B. Otto-Bliesner, J. Walsh, N.  
19 Bigelow, A. Hendricks, and K. Yoshikawa.: LGM permafrost distribution: how well can the  
20 latest PMIP multi-model ensembles perform reconstruction?. *Climate of the Past*. 9, 4. 2013.

21 Schaefer K., Zhang T., Bruhwiler L., Barrett AP.: Amount and timing of permafrost carbon  
22 release in response to climate warming. *Tellus*. Doi: 10.1111/j.1600-0889.2011.00527.x.  
23 2011.

24 Schmitt, J., Schneider, R., Elsig, J., Leuenberger, D., Laurantou, A., Chappellaz, J., Kohler,  
25 P., Joos, F., Stocker, T.F., Leuenberger, M. and Fischer, H.: Carbon isotope constraints on the  
26 deglacial CO<sub>2</sub> rise from ice cores. *Science*, 336(6082), 711-714, 2012.

27 Schneider von Diemling, T., Meinhausen, M., Levermann, A., Huber, V., Frieler, K.,  
28 Lawrence, D.M., Brovkin, V.: Estimating the near-surface permafrost-carbon feedback on  
29 global warming. *Biogeosciences*. 9, 649-665. 2012

1Schuur, E.A.G., Bockheim, J., Canadell, J.G., Euskirchen, E., Field, C.B., Goryachkin, S.V.,  
2Hagemann S., et al.: Vulnerability of permafrost carbon to climate change: Implications for  
3the global carbon cycle. *BioScience* 58, 8, 701-714. 2008.

4Schuur EAG., Vogel JG., Crummer KG., Lee H., Sickman JO., Osterkamp TE.: The effect of  
5permafrost thaw on old carbon release and net carbon exchange from tundra. *Nature*. 459. doi:  
610.1038/nature08031, 2009.

7Schuur, E. A.: High risk of permafrost thaw. *Nature*, 480, 32-33, 2011.

8Shakun, J. D., Clark, P. U., He, F., Marcott, S. A., Mix, A. C., Liu, Z., ... & Bard, E.: Global  
9warming preceded by increasing carbon dioxide concentrations during the last deglaciation.  
10*Nature*, 484(7392), 49-54, 2012.

11Sigman, D. M., Hain, M. P., & Haug, G. H.: The polar ocean and glacial cycles in  
12atmospheric CO<sub>2</sub> concentration. *Nature*, 466(7302), 47-55, 2010.

13Stocker, T.F., D. Qin, G.-K. Plattner, M. Tignor, S.K. Allen, J. Boschung, A. Nauels, Y. Xia,  
14V. Bex and P.M. Midgley (eds.), IPCC, 2013: Climate Change 2013: The Physical Science  
15Basis. Contribution of Working Group I to the Fifth Assessment Report of the  
16Intergovernmental Panel on Climate Change Cambridge University Press, Cambridge, United  
17Kingdom and New York, NY, USA, 1535 pp, 2013.

18Taras B., Sturm M., Liston GE. 2002: Snow-ground interface temperatures in the Kupuruk  
19River Basin, Arctic Alaska: measurements and model. *Journal of Hydrometeorology*. 3: 377-  
20394, 2002.

21Tarnocai C., Canadell JG., Schuur EAG., Kuhry P., Mazhitova G., Zimov S.: Soil organic  
22carbon pools in the northern circumpolar permafrost region. *Global Biogeochemical Cycles*.  
2323. GB2023. Doi: 10.1029/2008GB003327, 2009.

24van Huissteden J., Dolman AJ.: Soil carbon in the Arctic and the permafrost carbon feedback.  
25*Environmental Sustainability*. 4: 545-551, 2012.

26Vandenberghe J., Renssen H., Roche DM., Goosse H., Velichko AA., Gorbunov A.,  
27Levavasseur G.: Eurasia permafrost instability constrained by reduced sea-ice cover.  
28*Quaternary Science Reviews*. 34: 16-23. doi: 10.1016/j.quascirev.2011.12.001, 2012.

29Vavrus S.: The role of terrestrial snow cover in the climate system. *Climate Dynamics*. 29:  
3073-88. doi: 10.1007/s00382-007-0226-0, 2007.

1Wadham, J. L., S. Arndt, S. Tulaczyk, M. Stibal, M. Tranter, J. Telling, G. P. Lis et al.:  
2Potential methane reservoirs beneath Antarctica. *Nature* 488, 7413, 633-637. 2012.

3Wania R., Ross I., Prentice IC.: Intergrated peatlands and permafrost into a dynamic global  
4vegetation model: 1. Evaluation and sensitivity of physical land surface processes. *Global*  
5*Biogeochemical Cycles*. 23. GB3014. Doi: 10.1029/2008GB003412, 2009a.

6Wania R., Ross I., Prentice IC.: Intergrated peatlands and permafrost into a dynamic global  
7vegetation model: 2. Evaluation and sensitivity of vegetation and carbon cycle processes. 23.  
8GB3015. Doi: 10.1029/2008GB003413, 2009b.

9Willerslev, E., Davison, J., Moora, M., Zobel, M., Coissac, E., Edwards, M.E., Lorenzen,  
10E.D., et al.: Fifty thousand years of Arctic vegetation and megafaunal diet. *Nature*, 506, 7486  
1147-51. 2014.

12Yu, Z., Loisel, J., Brosseau, D. P., Beilman, D. W., & Hunt, S. J.: Global peatland dynamics  
13since the Last Glacial Maximum. *Geophysical Research Letters*, 37(13), 2010.

14Zech, R., Huang, Y., Zech, M., Taroza, R., and Zech, W.: High carbon sequestration in  
15Siberian permafrost loess-paleosols during glacials. *Climate of the Past*, 7, 2. 2011.

16Zhang T.: *Global Annual Freezing and Thawing Indices*. Boulder, Colorado USA: National  
17Snow and Ice Data Center, 1998.

18Zhang T.: Influence of the seasonal snow cover on the ground thermal regime. An overview.  
19*Reviews of Geophysics*. 43. RG4002. Doi: 8755-1209/05/2004RG000157, 2005.

20Zhang T., Heginbottom JA., Barry RG., Brown J.: Further statistics on the distribution of  
21permafrost and ground ice in the Northern Hemisphere. *Polar Geography*. 24:2, 126-131. doi  
2210.1080/10889370009377692, 2000.

23Zhao, M., Running, S., Heinsch, F. A., & Nemani, R.: MODIS-derived terrestrial primary  
24production. In *Land Remote Sensing and Global Environmental Change* (pp. 635-660).  
25Springer New York, 2011.

26Zimov NS., Zimov SA., Zimova AE., Zimova GM., Chuprynin VI., Chappin III FS.: Carbon  
27storage in permafrost and soils of the mammoth tundra-steppe biome: Role in the global  
28carbon budget. *Geophysical Research Letters*. 36. L02502. Doi: 10.1029/2008GL036332,  
292009.



1Zimov, S. A., Zimov, N. S., Tikhonov, A. N., & Chapin III, F. S.: Mammoth steppe: a high-  
2productivity phenomenon. *Quaternary Science Reviews*, 57, 26-45, 2012.

1Table 1. Simulated climates used in this study.

Date	Event
LGM (equilibrium)	Obtained after an 80kyr spin-up with glacial CO <sub>2</sub> levels of 190ppmv, reduced ocean volume, LGM ice sheets, LGM insolation, LGM runoff. Carbonate compensation in the ocean (Brovkin et al. 2002). Sea-level effects on coast lines are not included, land area is as PI (equilibrium). The continental shelves exposed at LGM are not accounted for in this model set-up because the fate of any carbon that may have accumulated on these shelves is not well constrained. The long time of spin-up, 80kyr, is required to allow the soil carbon pools to equilibrate.
PI (equilibrium)	Obtained after 40kyr spin-up with pre-industrial CO <sub>2</sub> levels of 280ppmv, present-day ocean volume, present-day ice sheets, insolation, and land run-off. The 40kyr spin-up time allows soil carbon pools to equilibrate.
PI (transient)	End of a 21kyr simulation of a transient deglaciation that has the LGM equilibrium climate as a start point at 21kyr BP. The PI (transient) is the climate at 0yr BP. The transient deglaciation has evolving ice sheets scaled to sea-level, increasing ocean volume, insolation changes (seasonality), carbonate compensation and LGM runoff. This transient PI climate is required to account for the long time to equilibrium of the permafrost affected soil carbon pools. In order to compare model output with ground-data the PI(transient) provides a more realistic model output.

1Table 2: permafrost area model settings for eq. (5)

	A	$\beta$
HIGH	0.58	$22(F_{sc} - 0.58)$
MED	0.555	$21(F_{sc} - 0.59)$
LOW-MED	0.54	$20.5(F_{sc} - 0.595)$
LOW	0.53	$20(F_{sc} - 0.6)$

2

1Table 3: selected settings for permafrost decomposition function, where subscript indicates  
2the soil pool. Permafrost area model is LOW-MEDIUM for all.

Constants settings for eq. (3)				
Dynamic settings	$a_{\text{fast}}$	$b_{\text{fast}}$	$a_{\text{slow}}$	$b_{\text{slow}}$
Slow	10	10	10	10
Medium	20	40	1	3
Fast	60	50	0	1
Xfast	60	80	0.1	0.1

3

1 Table 4: Modelled permafrost-affected land area and data based estimates

Permafrost area ( $\times 10^6 \text{ km}^2$ )			
(land underlain by permafrost)			
Permafrost area setting	model Pre-Industrial climate (equilibrium)	Pre-Industrial climate (transient)	Glacial climate
LOW-MEDIUM	14.0	18.4	20.7
Data estimate	12.21 to 16.98 (Zhang et al. 2000)		33.8 (Levvasseur et al. 2011)
			40 (Vandenberghe et al. 2012)

2

1

Period	Total land carbon (GtC)	Active land carbon (GtC)	Inert land carbon (GtC)
Present-day	3970+-325	2370+-125	1600+-300
LGM	3640+-400	1340+-500	2300+-300

2Table 5: Total land carbon stock estimates from Ciais et al. (2012)

3

Soil type	depth		Soil carbon (GtC)
Gelisols	To 1m	Turbels	211.9
		Orthels	51.3
		Histels	88.0
		All	351.5
	To 3m	Turbels	581.3
		Orthels	53.0
		Histels	183.7
		All	818.0
All soils	To 1m		495.8
	<b>To 3m</b>		<b>1024.0</b>
Pleistocene loess	<b>&gt;3m</b>		<b>407</b>
Deltaic	<b>&gt;3m</b>		<b>241</b>

2Table 6: Permafrost region soil carbon stock estimates from Tarnocai et al. (2009)

1Table 7: Modelled total land carbon stocks per model setting

Total land carbon (GtC)	Standard model	With permafrost, per dynamic setting			
		slow	medium	fast	xfast
PI (transient)	2199	4052	4425	4079	3819
LGM (eq)	1480	3597	3563	3467	3481

2

3



1Table 8: Modelled permafrost-region extra land carbon stocks wrt. standard model per model  
2setting

Extra soil carbon (GtC)	Standard model	With permafrost, per dynamic setting			
		slow	medium	fast	xfast
PI (transient)	0	1853	2226	1880	1620
LGM (eq)	0	2117	2083	1987	2001

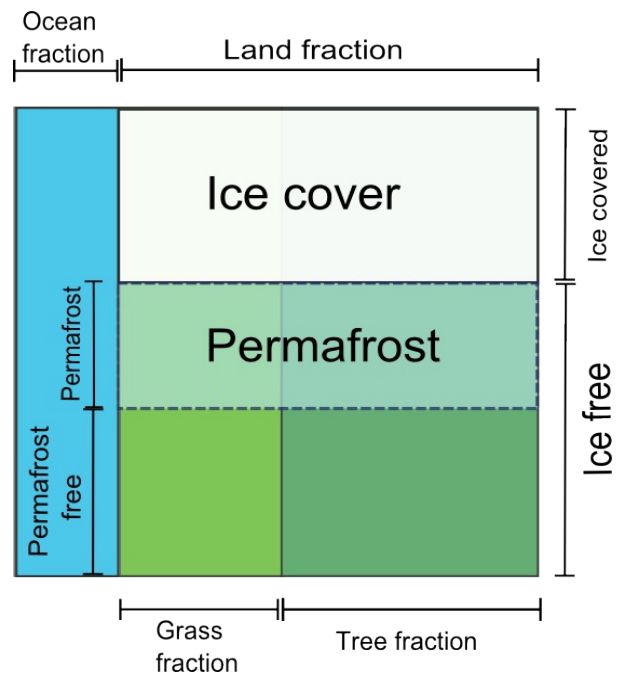
3

4

1Table C1: All settings for eq. (3) (main article) used to tune total land carbon and permafrost-  
2carbon dynamics.

Area: LOW						Area: MED				
	a fast	b fast	a slow	b slow			a fast	b fast	a slow	b slow
1	30	30	2	2		1	50	40	0	0.5
2	40	30	2	2		2	20	20	2	2
3	50	50	2	2		3	10	10	10	10
4	50	50	3	3		4	30	50	0	0.5
5	20	20	10	10		5	60	50	0	1
6	10	10	20	20						
7	55	45	3	2		Area: HIGH				
8	70	60	0	1			a fast	b fast	a slow	b slow
9	60	70	2	2		1	30	30	2	2
10	80	70	0	1		2	15	30	1	2
11	100	90	0	1		3	15	15	15	15
12	150	100	0	0.5		4	10	30	0	1
13	100	150	0	0.5		5	5	45	0	2
14	75	200	0	0.5		6	4	8	12	16
15	20	20	2	2		7	8	35	0	1
16	60	50	0	1		8	3	8	12	16
						9	1	35	1	2
Area: LOW-MED						10	30	10	1	1
	a fast	b fast	a slow	b slow		11	0.5	40	0.5	2.5
1	50	40	0	0.5		12	3	7	11	15
2	21	20	2	2		13	0.2	45	0.2	3
3	10	10	10	10		14	1	100	0	1
4	60	50	0	1		15	20	30	0	1
5	50	60	0	1		16	70	40	0	0.5
6	10	30	1	3		17	20	20	2	2
7	20	40	1	3		18	60	50	0	1
8	5	50	1	3						
9	30	70	0	1						
10	50	5	3	1						
11	45	30	3	2						
12	45	25	3	2						
13	40	20	3	2						
14	60	80	0.1	0.1						
15	10	40	1	4						
16	5	55	1	2						

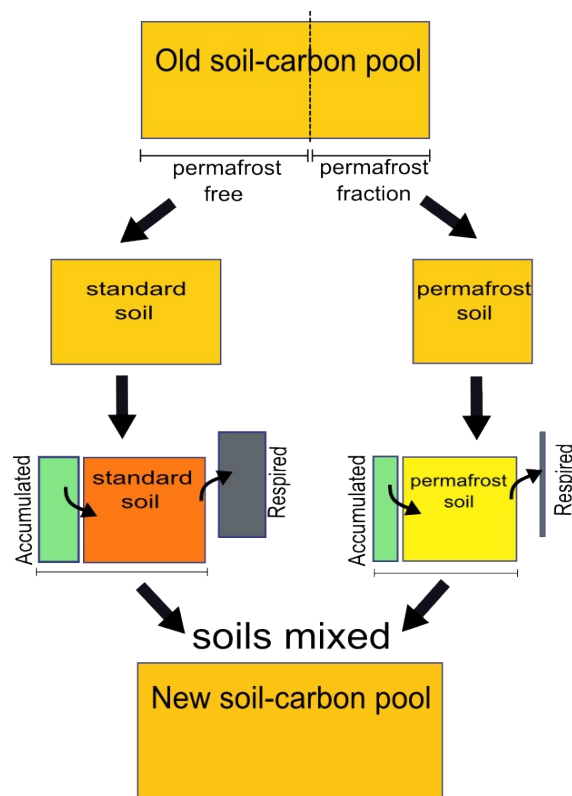
3



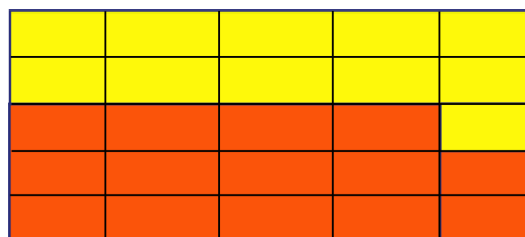
2

3Figure 1: A CLIMBER-2P grid cell showing the distribution of different cell cover types

4



a) Re-mixing model



for each sub-cell:



b) Sub-grid model

Figure 2: Schematic of a CLIMBER-2P grid cell showing how carbon is accumulated at each time-step. Re-mixing model a) separates grid cell into permafrost or non permafrost, calculates the change in carbon pool and re-mixing all carbon in the cell back together. Sub-grid model b) separates the grid cell into 25 sub-grid cells and calculates change in carbon pool in each individually and does not re-mix any carbon between sub-grid cells.

1

2

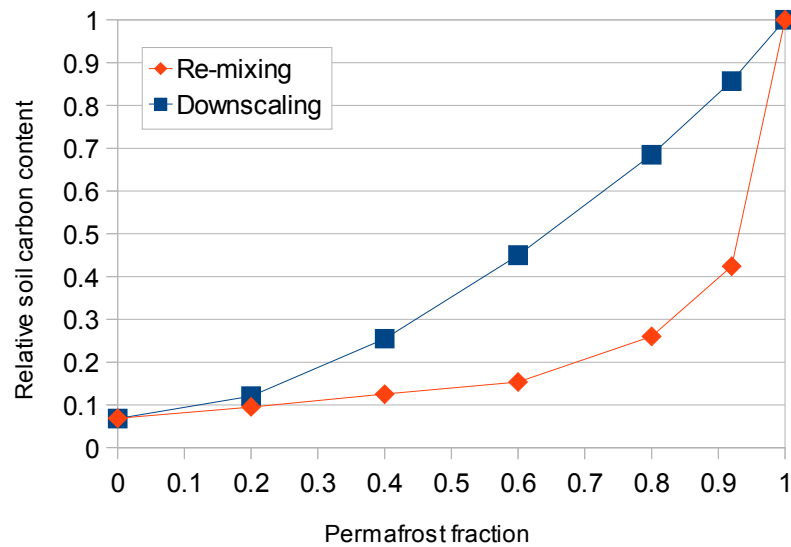
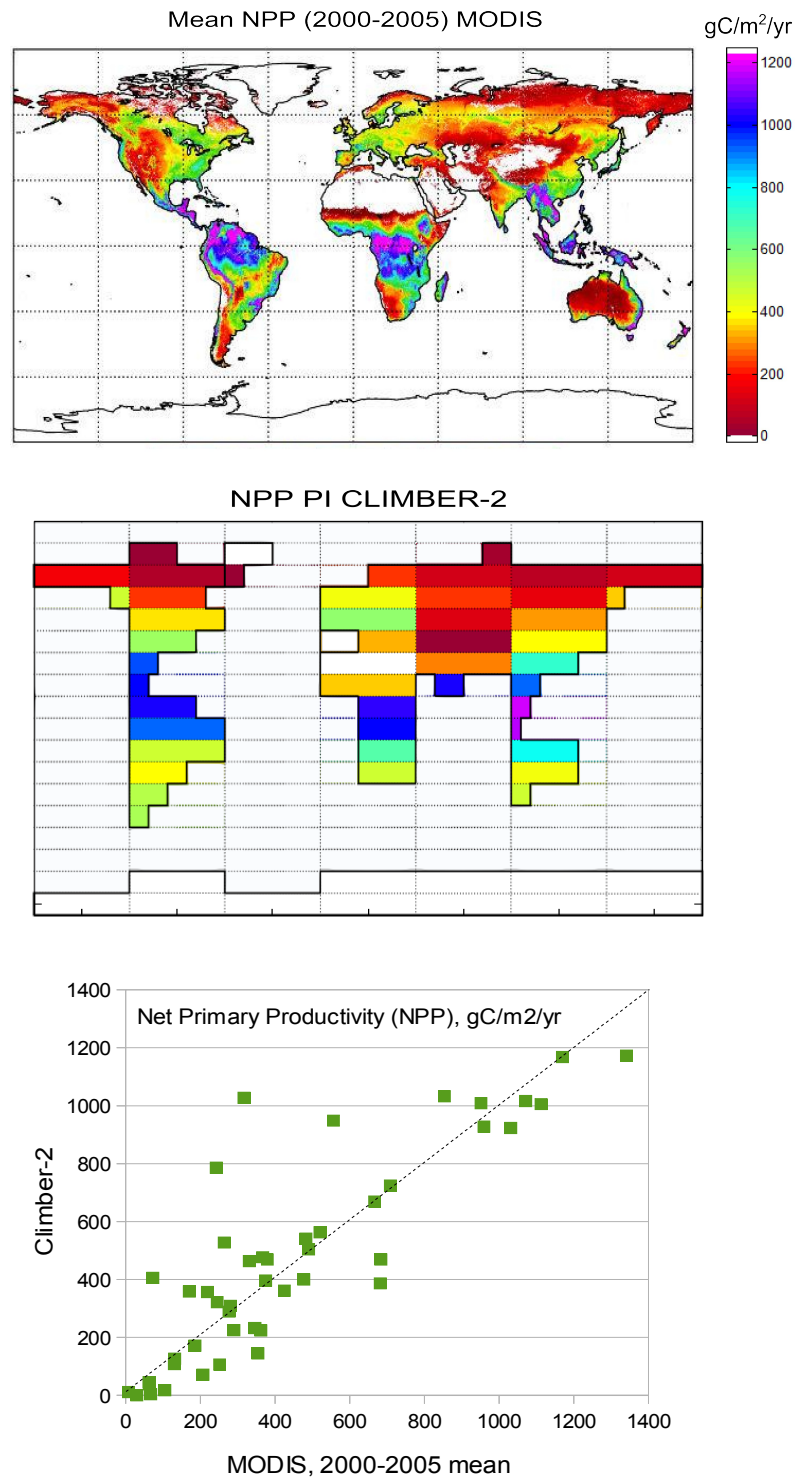


Figure 3: Comparison of sub-grid to re-mixing approach for relative soil carbon contents of a grid cell for increasing permafrost fraction. The variables of mean annual temperature and frost-index vary with permafrost fraction according to data relationships upscaled to CLIMBER-2 grid relationships (see Appendix A and figure A2).



2Figure 4: Comparison of NPP (net primary productivity), which has a control on carbon input  
3to soils, for MODIS dataset (top, mean 2000-2005) and CLIMBER-2 model for PI(eq)  
4(modelled year 1950) plotted on the same scale (gC/m<sup>2</sup>/yr). MODIS data upscaled to  
5CLIMBER-2 grid scale shown against equivalent points for CLIMBER-2 NPP.

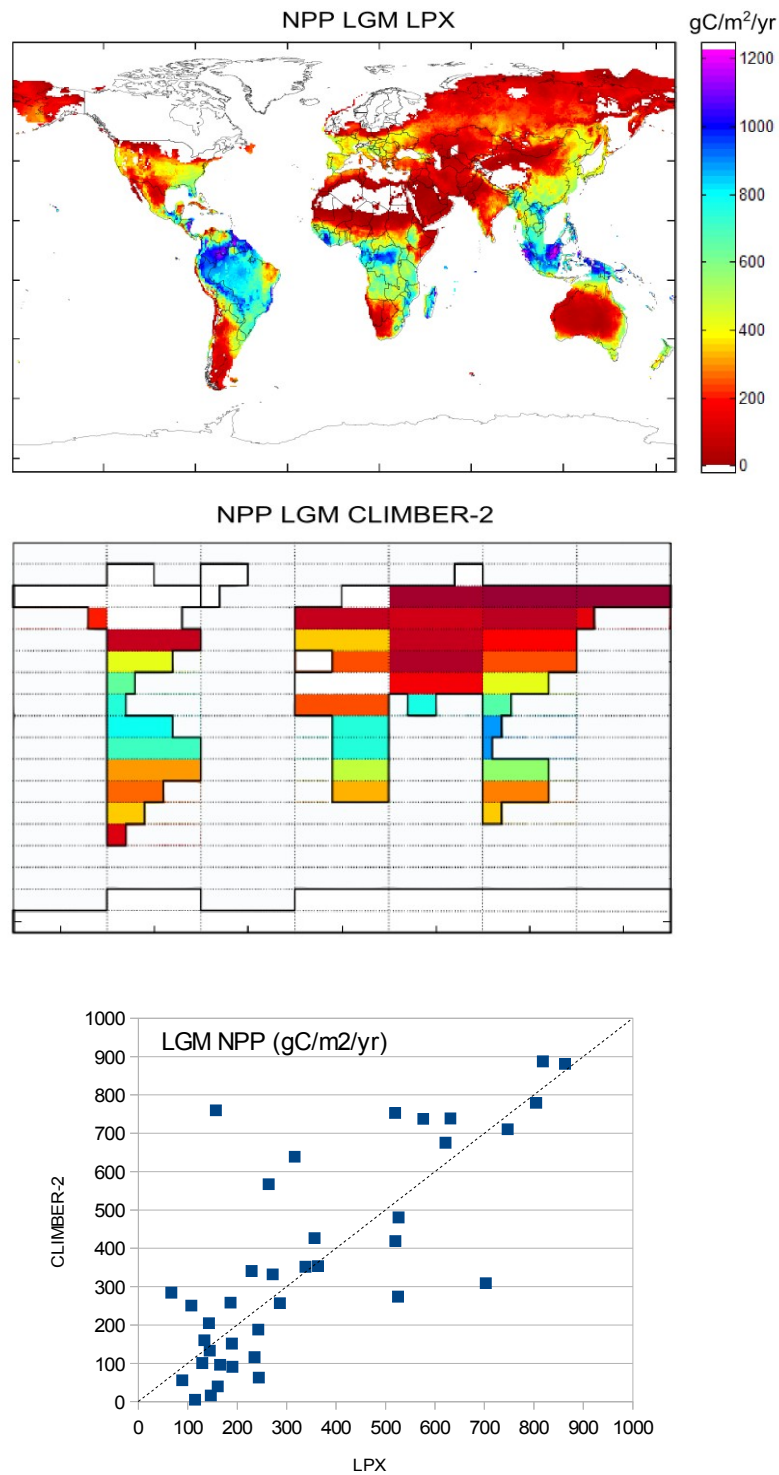
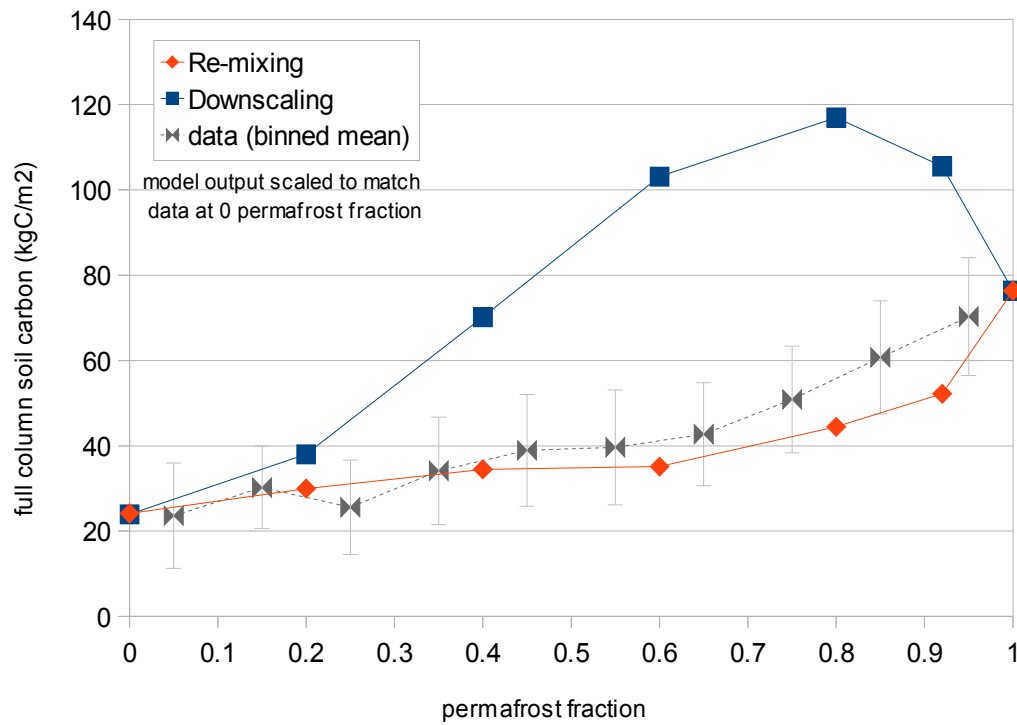


Figure 5: Comparison of NPP (net primary productivity), which has a control on carbon input to soils, for LPX model (top, courtesy M Martin-Calvo, average of an ensemble model output) and CLIMBER-2 model for LGM(eq) (at 21kyr BP) plotted on the same scale ( $\text{gC/m}^2/\text{yr}$ ), and same scale as figure 5. LPX output upscaled to CLIMBER-2 grid and plotted against equivalent CLIMBER-2 NPP shown also.

1



3

Figure 6: Modelled output for 1D models along a permafrost gradient, with correction for 5NPP and initial value (at 0% permafrost). Overlaid on 1degree data for socc binned into 0.1 6permafrost fraction mean values  $\pm 1$  sigma (Hugelius et al 2013) permafrost fraction is 7calculated using relationship identified in section 3.2.

8



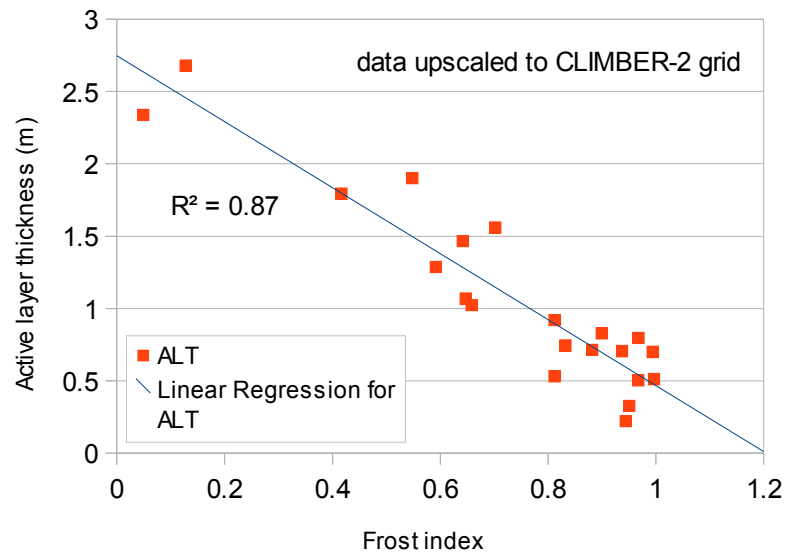


Figure 7: Measurement data for active layer thickness (CALM network, Brown et al. 2003) and Frost index (Zhang et al. 1998) upscaled to the CLIMBER-2 grid scale, showing the distinct relationship of reducing active layer with increasing frost index at this scale. Note, permafrost-fraction is calculated from frost-index in our model (section 3.2 main text).

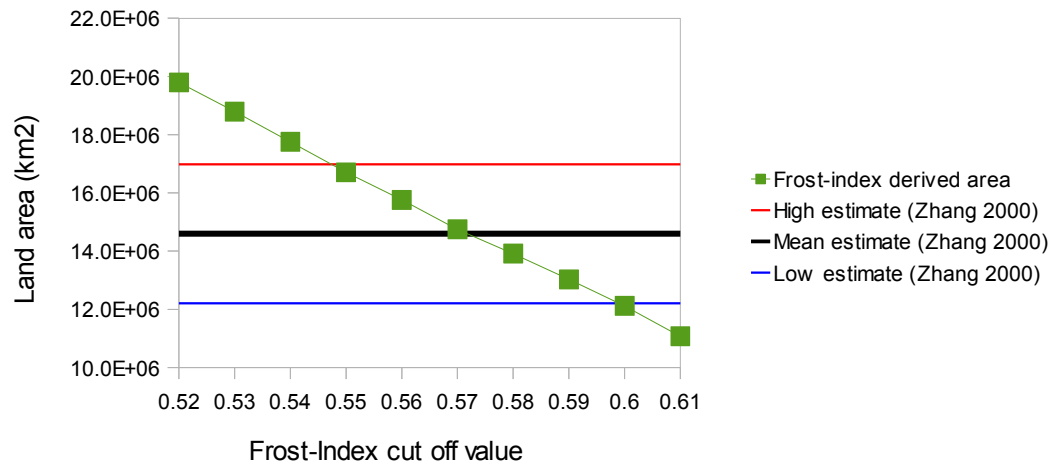


Figure 8: Total land area with a frost-index higher (colder) than the x-axis cut-off value, for frost-index data from Zhang et al 1998 (NSIDC). Shown in horizontal lines are the Zhang 2000 data estimates for area of land underlain by permafrost.

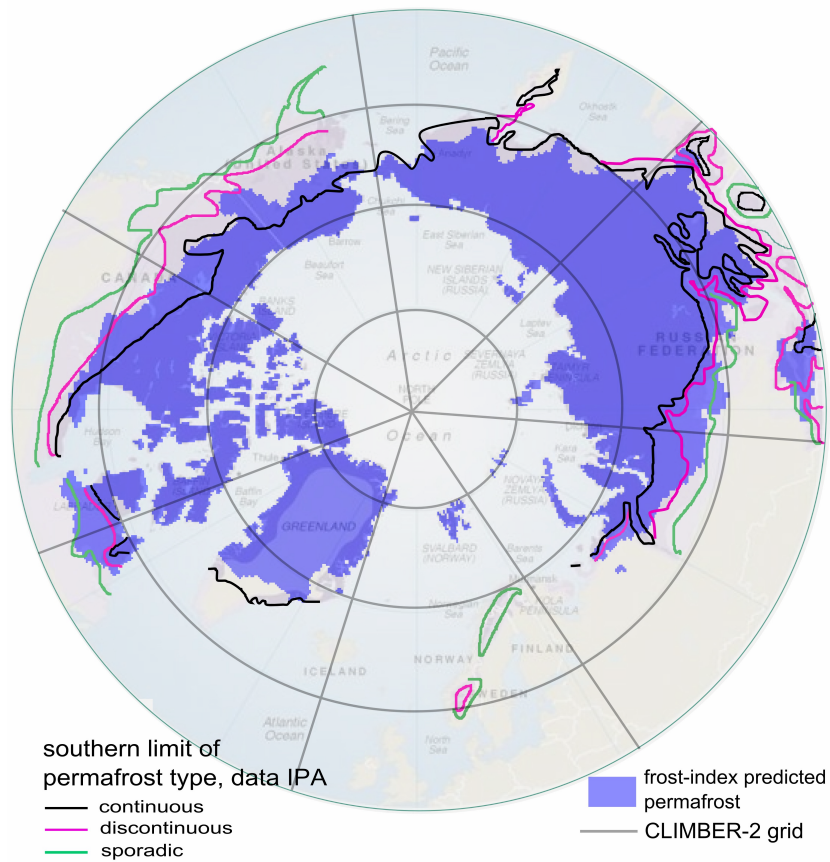


Figure 9: Map of land with frost-index greater than 0.57 (frost-index predicted permafrost) shown in blue with southern limit of permafrost boundaries for the present day defined by IPA overlaid. Black line: continuous permafrost, pink line: discontinuous permafrost, green line: sporadic permafrost. Grey lines are the CLIMBER-2 grid.

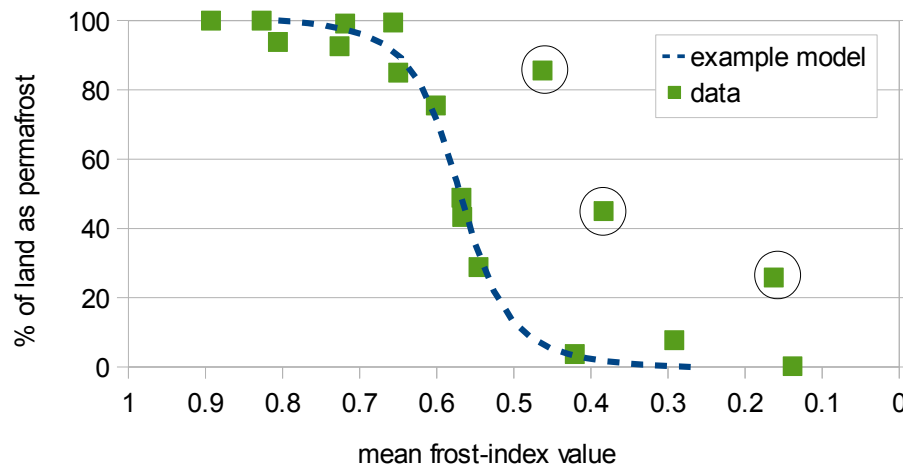


Figure 10: Frost-index predicted permafrost fraction of land from figure 8 upscaled to the CLIMBER-2 grid and plotted against mean Frost-index for the same CLIMBER-2 grid cell. Circled points are where the total fraction of land vs ocean in the grid cell is small (land is less than 25% of the grid cell) and ocean temperatures pull frost-index lower (warmer). Blue dashed line is a representative relationship between frost-index and permafrost land-fraction.

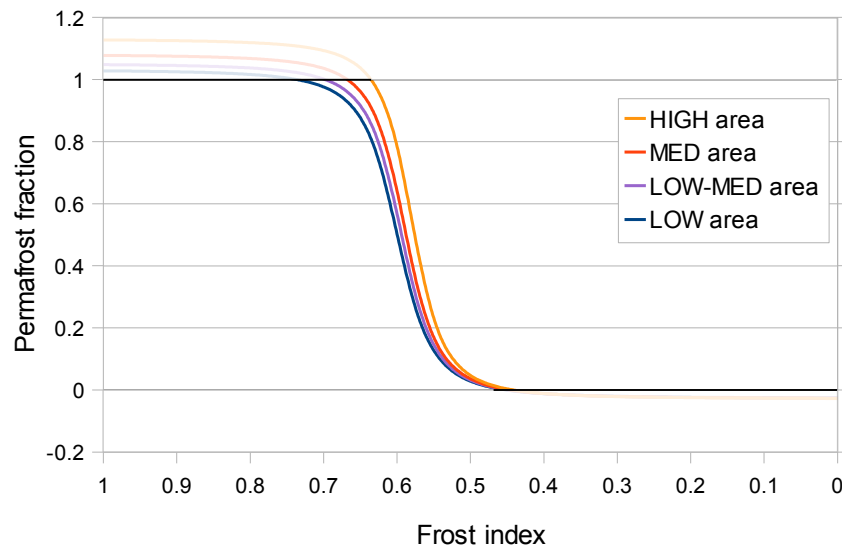


Figure 11: CLIMBER-2P model for permafrost-fraction of the land in a grid cell from frost-index (snow corrected). Range of areas are within the range of estimates for present-day land area underlain by permafrost by Zhang et al. (2000). Permafrost fraction is limited between 0 and 1. Zhang estimate for total permafrost area is  $12.21$  to  $16.98 \times 10^6 \text{ km}^2$ . Listed from HIGH to LOW model output is:  $16.35$ ,  $14.87$ ,  $14.00$  and  $13.21 \times 10^6 \text{ km}^2$ .

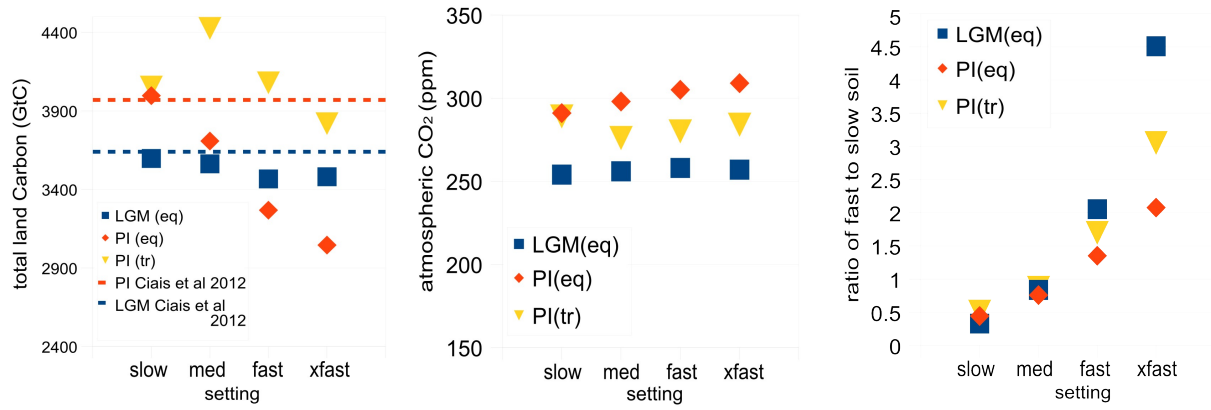
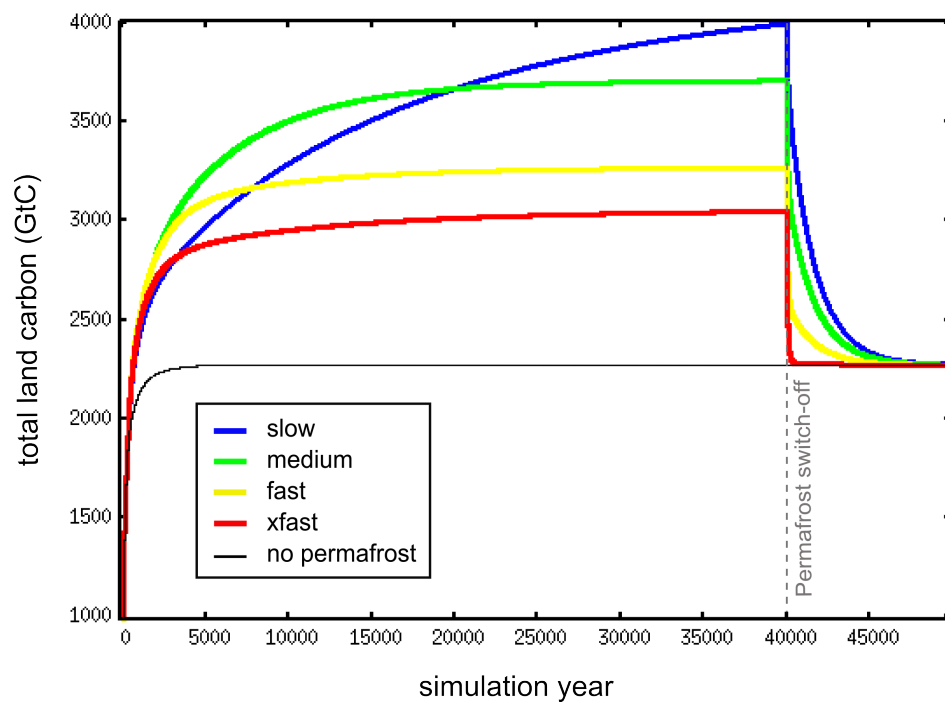


Figure 12: Chosen dynamic settings for the range of permafrost-carbon dynamics. Left: total land carbon with Ciaia et al. (2012) estimates as dashed lines. Middle: atmospheric CO<sub>2</sub> (ppm). Right: ratio of all fast to all slow soil pools indicating the speed of response of the soil carbon to changing climate.

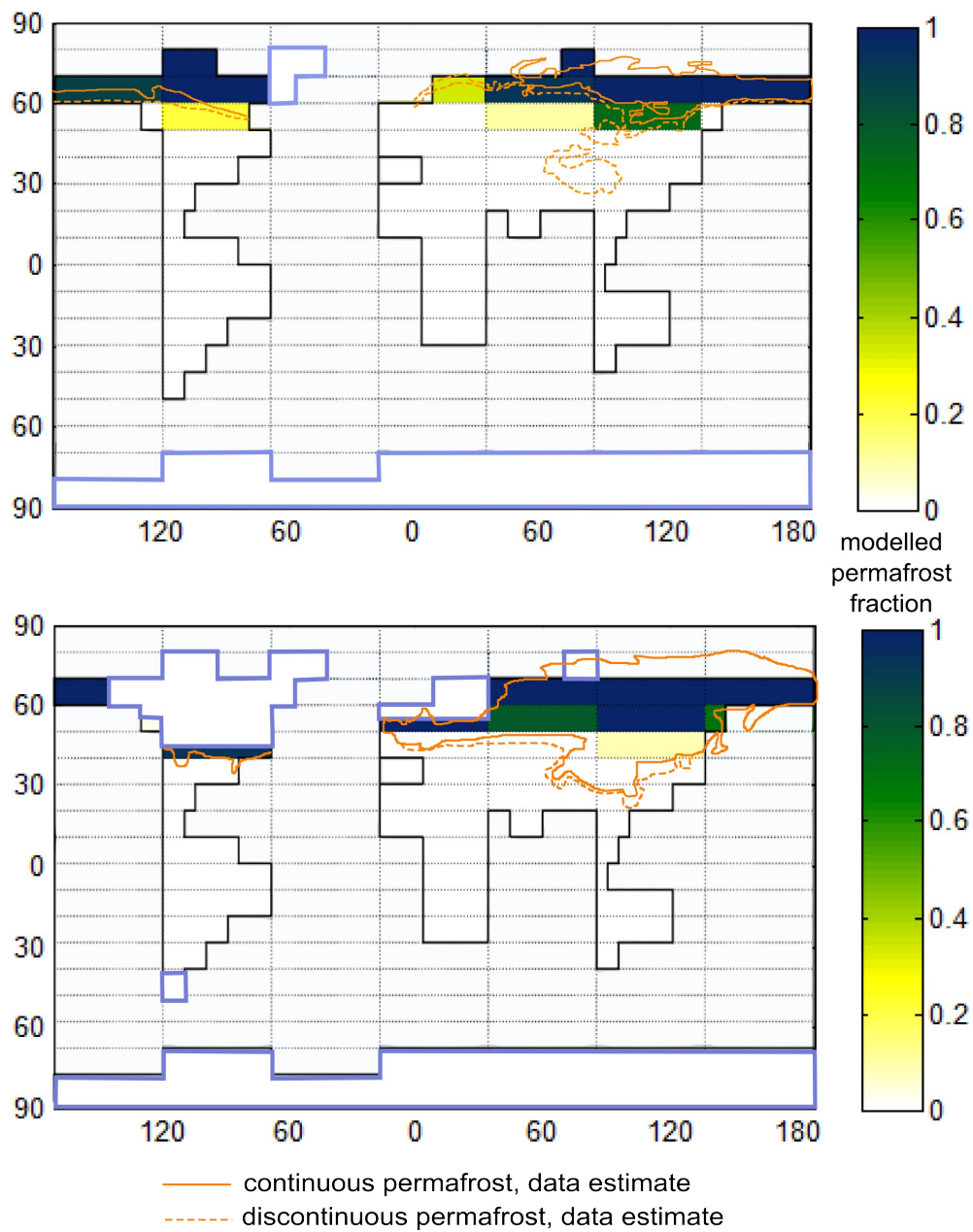
1



3

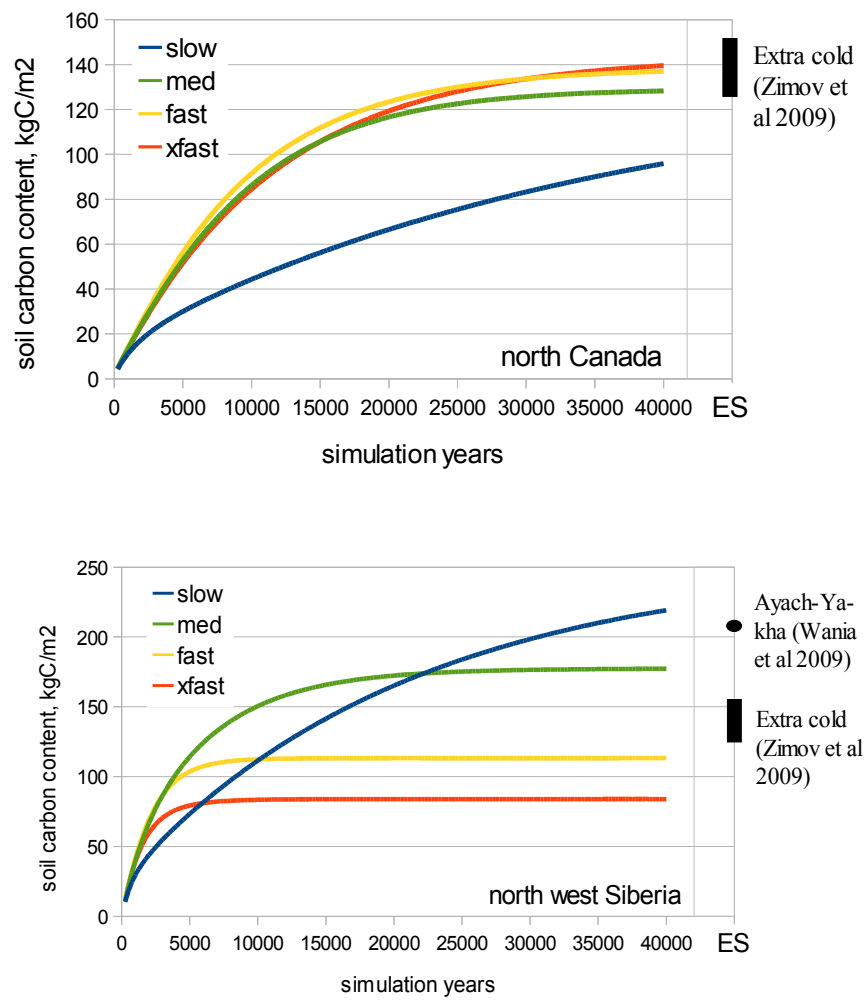
4Figure 13: Total land carbon (GtC) for the PI(eq) simulation followed by a permafrost switch-  
 5off at 40k simulation years representing a complete and immediate permafrost thaw  
 6demonstrating the different dynamic behaviour of each dynamic setting.

7



2Figure 14: Modelled permafrost area for a): PI(tr) simulation, b) LGM(eq) simulation for 3LOW-MEDIUM permafrost area. Overlaid in orange are data estimates from Circumpolar 4Atlas (Jones et al. 2009) for present-day, Vandenberghe et al. (2008) for LGM Eurasia, 5French and Millar (2013) for LGM N. America.

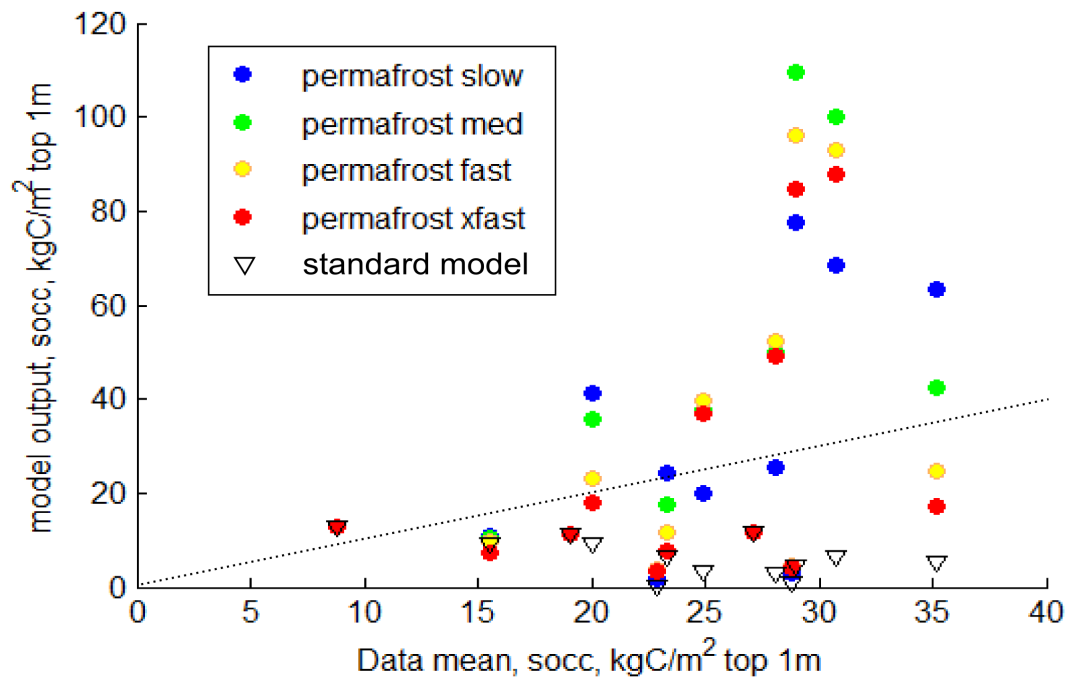




2Figure 15: modelled PI(eq) simulation output for total soil column carbon content for two grid  
3cells. ES is equilibrium state (>50kys)

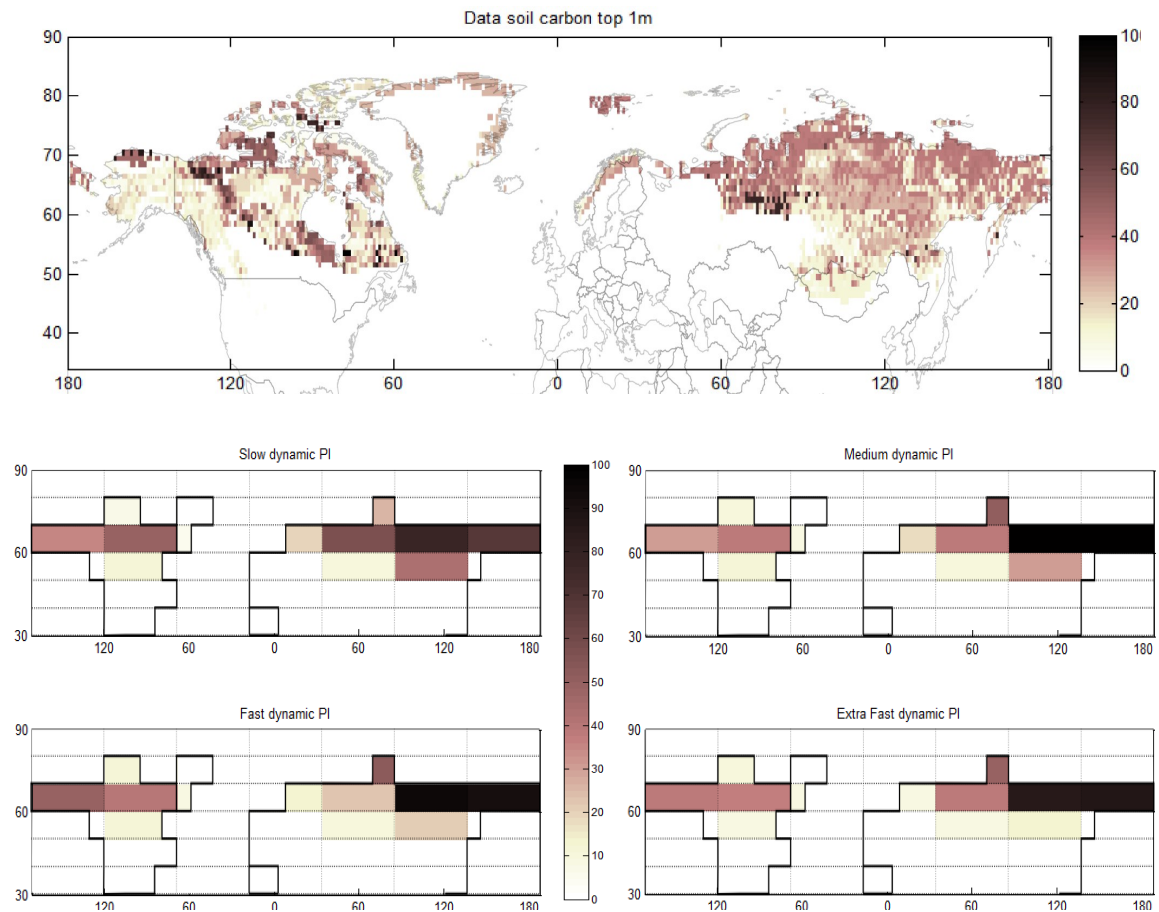
4

1  
2  
3



5Figure 16: Modelled socc (soil organic carbon content, kgC/m<sup>2</sup>) for the top 1m plotted against  
6socc data for the top 1m of soil upscaled to the CLIMBER-2 grid scale. Circles are for  
7permafrost-carbon model (CLIMBER-2P), triangles are for the standard model (CLIMBER-  
82). Dashed line shows the 1:1 position. Points are socc kgC/m<sup>2</sup>

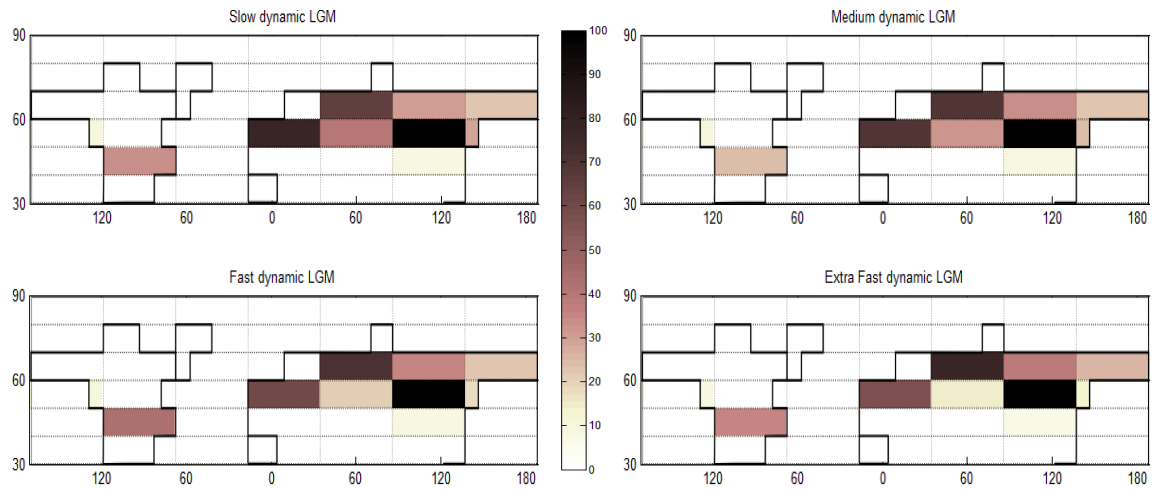
9



1Figure 17: Socc (soil organic carbon content) data ( $\text{kgC}/\text{m}^2$ ) for the top 100cm of soils,  
2Hugelius et al. (2013) (top). Modelled PI(tr) socc ( $\text{kgC}/\text{m}^2$ ) in permafrost soils for top 100cm  
3(lower four).

4

1

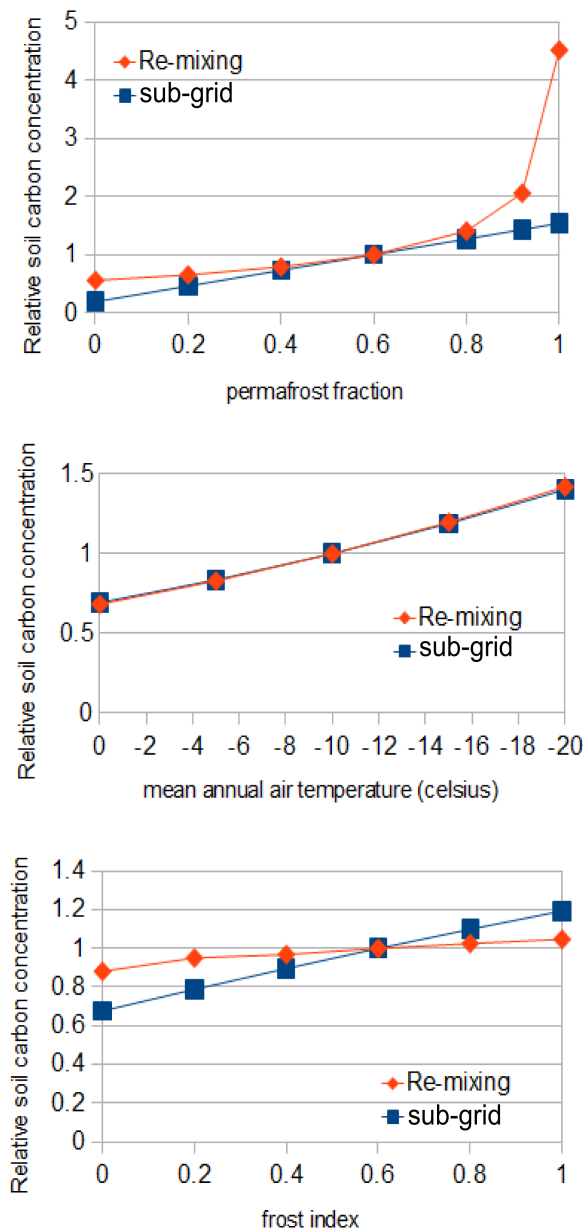


2Figure 18: Modelled LGM(eq) socc (kgC/m<sup>2</sup>) in permafrost soils for top 100cm.

3

4

5



2Figure A1: 1D model output to compare the performance of the re-mixing (diamonds) and the  
3sub-grid (squares) approaches. Top: MAT (mean annual temperature) and frost-index are  
4constant, permafrost-fraction is variable. Middle: frost-index and permafrost-fraction are  
5constant, MAT is variable. Bottom: permafrost-fraction and MAT are constant, frost index is  
6variable. Input to soils from plant mortality and rainfall are constant for all.

7

8

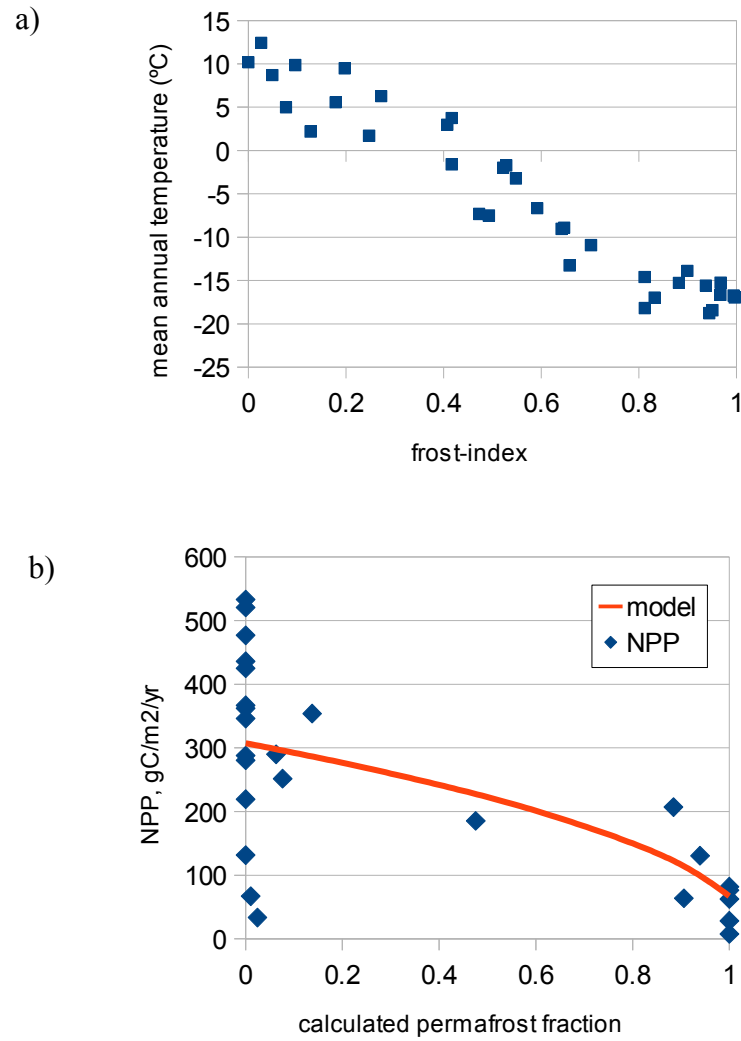
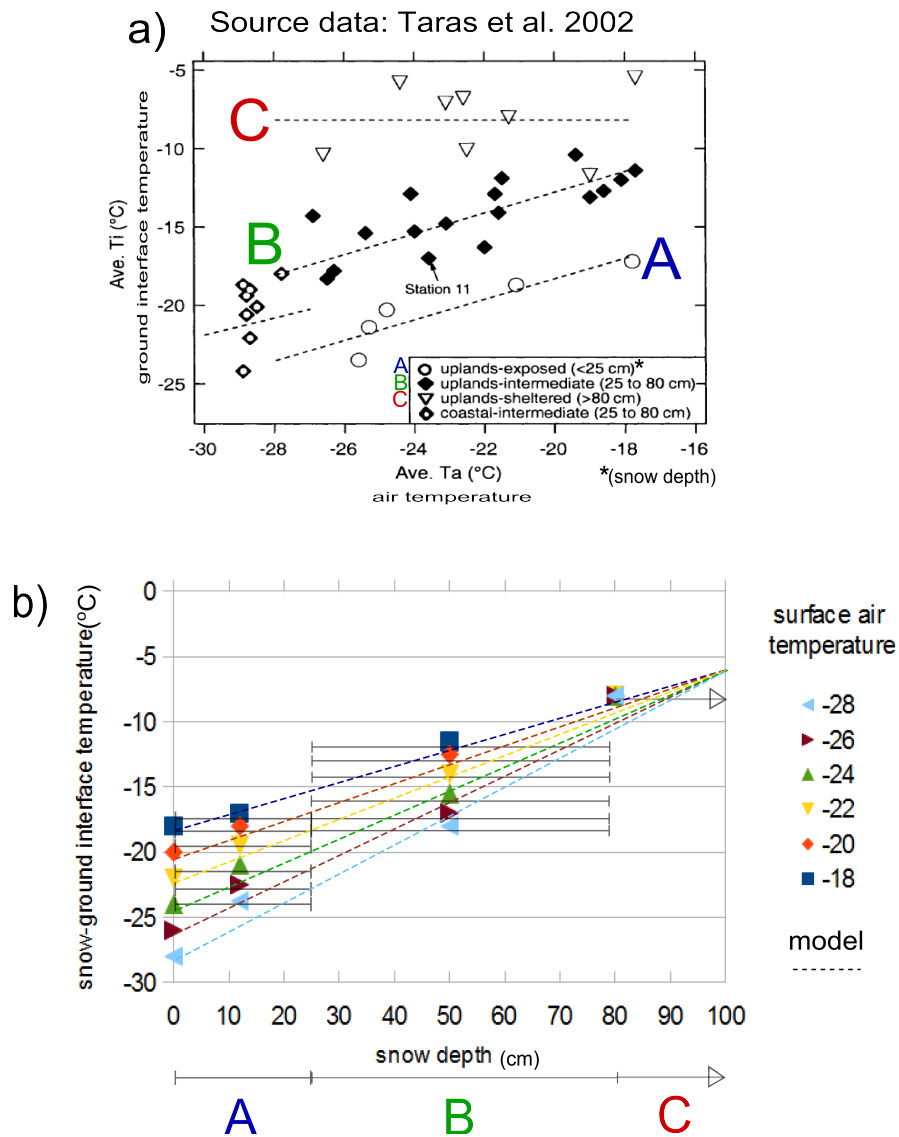


Figure A2: relationships between frost-index and mean annual temperature on the CLIMBER-32 grid scale (data from Zhang et al 1998 and Jones et al 1999). Frost-index determines permafrost fraction according to model described in section 3.2 (main text). NPP data for the permafrost zone from MODIS plotted against permafrost fraction (calculated from frost index values of Zhang et al 1998) on the CLIMBER-2 grid scale.



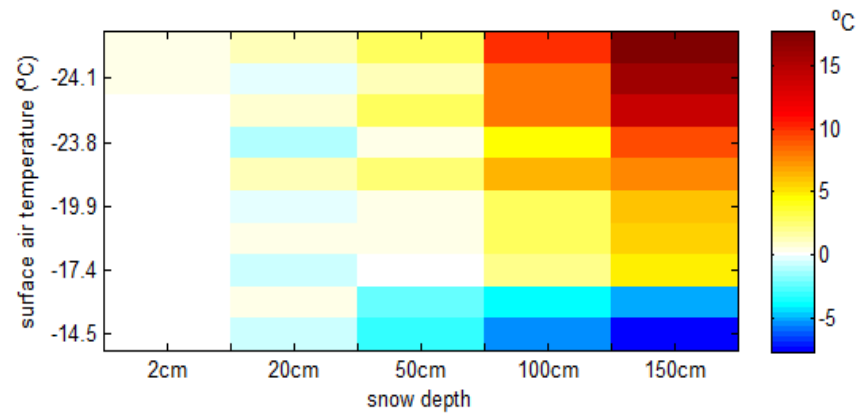
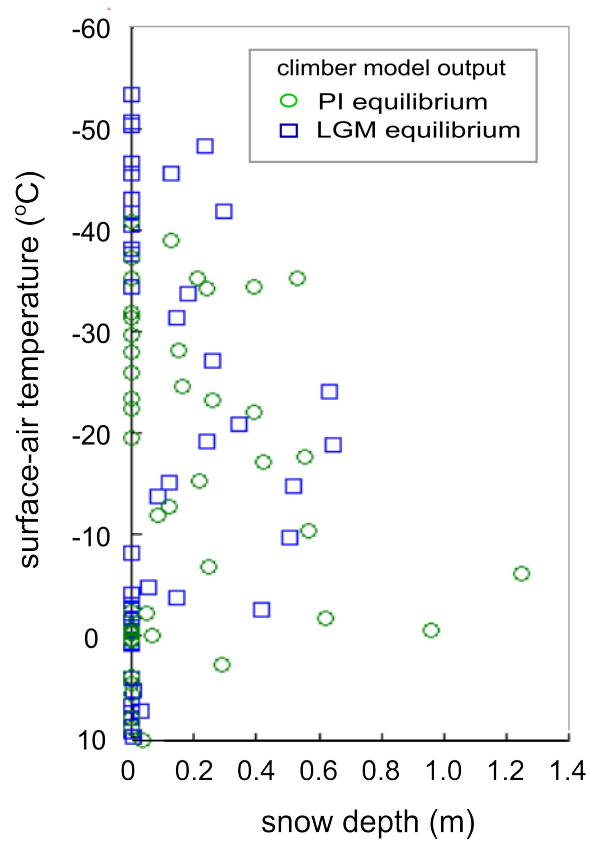


Figure B2: Model error when the linear snow correction model is used to predict temperatures at snow-depth or snow-ground interface for data from Morse and Burn 2010 (measurement data is down snow column temperatures). Positive numbers indicate the linear model output is too warm compared to data.



1



3

4Figure B3: CLIMBER-2 model output for snow depth (m) plotted against surface air  
5temperature (°C) for the PI(eq) (green circles) and LGM(eq) (blue squares) climates. Model  
6output does not show extreme conditions for snow cover due to the very large grid-cell size.

7

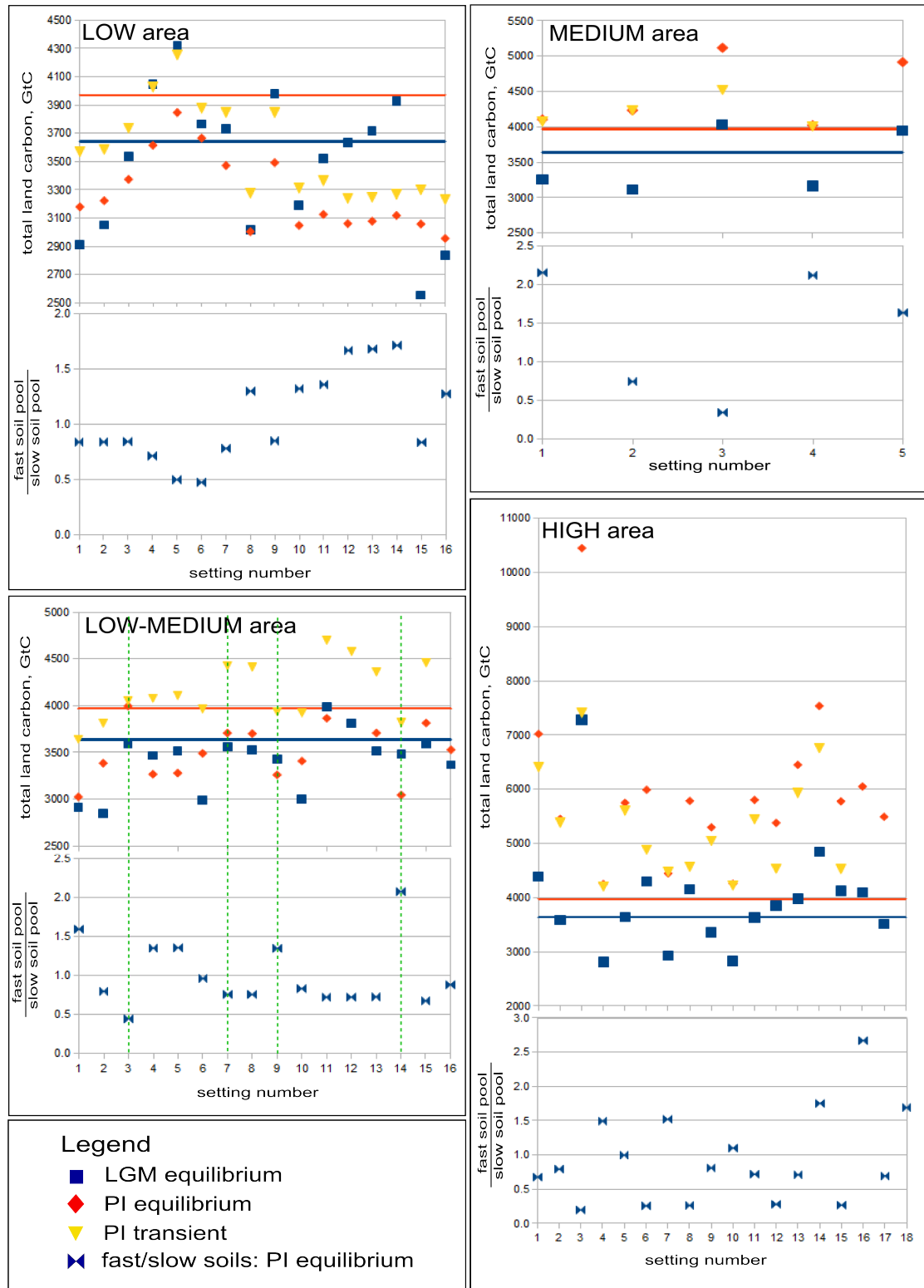


Figure C1: Modelled total land carbon stocks, and ratio of fast soils to slow soils for all settings used to tune the permafrost-carbon dynamics. Blue squares are for the LGM (eq) simulation, red diamonds are for the PI(eq) simulation and yellow triangles are for the PI(tr) simulation. Horizontal lines show the total land carbon estimates of Ciais et al. (2012). Green dashed lines indicate the chosen dynamic settings where LGM(eq) and PI(tr) show best agreement with Ciais et al estimates.